# Intraflagellar transport is required for the maintenance of the trypanosome flagellum composition but not length

Cécile Fort[1,2], Serge Bonnefoy[1], Linda Kohl[3] and Philippe Bastin[1,*]

[1]Trypanosome Cell Biology Unit, INSERM U1201, Institut Pasteur, 25 Rue du Docteur Roux, 75015 Paris, France

[2]Université Pierre et Marie Curie Paris 6, Cellule Pasteur-UPMC, 25 rue du docteur Roux, 75015 Paris

[3]Unité Molécules de Communication et Adaptation des Microorganismes (MCAM, UMR7245), Sorbonne Universités, Muséum National d'Histoire Naturelle, CNRS; CP52, 61 rue Buffon, 75005 Paris, France

* Author for correspondence pbastin@pasteur.fr

Keywords: intraflagellar transport, cilia and flagella, organelle construction and maintenance, trypanosome

## Summary statement

Intraflagellar transport is the machinery responsible for the construction of cilia and flagella. We show that **in trypanosomes** it is required for the maintenance of flagellum integrity but not of organelle length.

## Abstract

IntraFlagellar Transport (IFT) is required for construction of most cilia and flagella. Here we used electron microscopy, immunofluorescence and live video-microscopy to show that IFT is absent or arrested in the mature flagellum of *Trypanosoma brucei* upon RNAi knockdown of IFT88 and IFT140 respectively. Flagella assembled prior to RNAi did not shorten showing that IFT is not essential for length maintenance. While the ultrastructure of the axoneme was not visibly affected, flagellar beating was strongly reduced and the distribution of several flagellar components was drastically modified. The R subunit of the protein kinase A was no longer concentrated in the flagellum but was largely found in the cell body while the kinesin 9B motor was accumulating at the distal tip of the flagellum. In contrast, the distal tip protein FLAM8 was dispersed along the flagellum. This reveals that IFT also functions in maintaining the distribution of some flagellar proteins after construction of the organelle is completed.

## Introduction

Cilia and flagella (interchangeable terms) are found at the surface of eukaryotic cells where they perform multiple roles including cellular motility, sensory function, developmental signalling and cell morphogenesis (Drummond, 2012). They share a similar basic structure with an axoneme composed of nine doublets of microtubules surrounded by a specific membrane. During assembly of cilia and flagella, the incorporation of new subunits takes place at the distal end of the organelle. The construction relies on an evolutionary-conserved process called intraflagellar transport (IFT), a bi-directional movement of multi-protein complexes between the membrane and the axoneme microtubules (Kozminski et al., 1993). IFT particles or trains (Pigino et al., 2009) are composed of proteins that can be separated into a complex A and a complex B (Cole et al., 1998; Piperno and Mead, 1997). IFT proteins have been found along the length of cilia (mature or in construction), but a significant proportion is also found at the basal body area and in the cell body (Absalon et al., 2008; Cole et al., 1998; Deane et al., 2001; Pazour et al., 2002). Inside the flagellum, kinesin II **(a member of the kinesin-2 family of motors)** transports IFT-A and IFT-B complexes, the inactive IFT dynein motor (Blisnick et al., 2014; Hao et al., 2011a; Signor et al., 1999) and axonemal precursors from the base to the tip of flagellum (Craft et al., 2015; Wren et al., 2013). At the tip of the flagellum, axonemal components are delivered for assembly whereas IFT trains are remodelled and returned to the base by the active dynein motor (Buisson et al., 2013; Pedersen et al., 2006).

In agreement with this model, inhibition of IFT blocks the construction of cilia in all species investigated to date including algae (Kozminski et al., 1995; Pazour et al., 2000), nematodes (Haycraft et al., 2001; Signor et al., 1999), ciliates (Brown et al., 2003; Brown et al., 1999), mammals (Nonaka et al., 1998; Pazour et al., 2002), trypanosomes (Kohl et al.,

2003), insects (Lee et al., 2008; Sarpal et al., 2003) or fish (Sun et al., 2004). However, video-microscopy revealed that IFT remains active after assembly of the organelle in many cell types (Buisson et al., 2013; Kozminski et al., 1993; Orozco et al., 1999), implying the existence of functions beyond construction. The temperature sensitive *fla10 Chlamydomonas* mutant (Huang et al., 1977) was instrumental in revealing a function for IFT in the maintenance of flagellum length in this organism. *FLA10* encodes one of the motor subunits of the heterotrimeric IFT kinesin. At the permissive temperature, IFT takes place and flagella are assembled normally. Once the cells are shifted to the restrictive temperature, IFT ceases and flagella progressively shorten until they eventually disappear (Kozminski et al., 1995). This result was explained by elegant experiments using epitope-tagged tubulin revealing that the tip of the flagellum constantly depolymerises and that incorporation of fresh tubulin compensates for that phenomenon (Marshall and Rosenbaum, 2001). Hence, IFT would be required to ensure a constant input of tubulin to balance this loss. This does not happen anymore in *fla10* cells grown at the restrictive temperature, supporting a role of IFT in the maintenance of flagellum length (Marshall and Rosenbaum, 2001). However, formal evidence in other organisms is missing, probably because of the difficulty of discriminating cilium assembly from maintenance in mammalian cells or in *C. elegans*.

Here, we used the flagellated protist *Trypanosoma brucei* as a model to investigate the role of IFT in flagellum maintenance. It is responsible for sleeping sickness in central Africa but also turned out as an excellent model to study flagellum biology (Vincensini et al., 2011). It assembles a new flagellum at each cell cycle while conserving the old one (Sherwin and Gull, 1989a), providing the opportunity to compare mature and constructing flagella in the same cell. Its genome contains the full complement of IFT-A, IFT-B, kinesin and dynein genes with the only exception of the kinesin-associated protein (KAP)(Julkowska and Bastin, 2009). IFT has been imaged by tagging multiple IFT-B or dynein subunits and is active

during both construction and maintenance. The expression of various components of the IFT-A and IFT-B complexes has been individually silenced using inducible RNAi, resulting in failure of flagellum construction (Absalon et al., 2008; Adhiambo et al., 2009; Blisnick et al., 2014; Davidge et al., 2006; Franklin and Ullu, 2010; Huet et al., 2014; Kohl et al., 2003). Usually, inhibition of IFT-B proteins (for example IFT88) blocked axoneme construction in agreement with a default in anterograde transport whereas absence of IFT-A proteins (such as IFT140) led to formation of short flagella filled with IFT material, indicative of defects in retrograde transport (Absalon et al., 2008).

In all cases, flagella assembled before RNAi remained present, a phenomenon then interpreted as the persistence of IFT proteins and trafficking (Kohl et al., 2003). Indeed, RNAi destroys mRNA and therefore impacts only on new protein synthesis while existing proteins disappear according to their own turnover rate (Bastin et al., 2000). However, efficient tools to investigate IFT were not available at the time. We since produced a monoclonal antibody against the IFT-B protein IFT172 (Adhiambo et al., 2009) and set up conditions to reliably visualise IFT in trypanosomes (Buisson et al., 2013). Moreover, the development of vectors for *in situ* tagging now allows expression of fluorescent fusion proteins at their endogenous level, an essential condition to monitor IFT in mutant situations (Kelly et al., 2007). Therefore it is now possible to examine IFT status in mature flagella in an attempt to decipher the role of IFT in flagellum maintenance.

Using transmission electron microscopy (TEM), immunofluorescence assays (IFA) and live video-microscopy, we show that IFT is absent or arrested in old flagella of trypanosome *IFT88*$^{RNAi}$ (anterograde mutant) and *IFT140*$^{RNAi}$ (retrograde mutant), respectively. In these conditions, the old flagellum does not shorten but the distribution of several of its proteins is drastically modified, revealing a key function for IFT in the maintenance of flagellum composition.

## Results

### The amount of IFT particles is modified in existing flagella of IFT-A and IFT-B mutants

Previous experiments showed that depletion of IFT88 in the *IFT88*$^{RNAi}$ cell line blocks axoneme construction in agreement with a default in anterograde transport whereas absence of IFT140 in *IFT140*$^{RNAi}$ cell line leads to formation of short flagella filled with IFT material, indicative of defects in retrograde transport (Absalon et al., 2008; Kohl et al., 2003). Here we investigated the fate of IFT proteins and their trafficking in cells with long flagella that had been assembled prior to RNAi.

The presence of IFT particles in the old flagella of *IFT88*$^{RNAi}$ and *IFT140*$^{RNAi}$ cells was examined by transmission electron microscopy (TEM) in non-induced cells and in samples induced for two days. In these conditions, less than 10% of the cells still construct a new flagellum and when it happens, this flagellum is very short, rarely extends beyond the flagellar pocket and misses the paraflagellar rod (Absalon et al., 2008; Kohl et al., 2003). Therefore, sections through the flagellum in these samples will overwhelmingly correspond to the old flagellum. IFT particles are recognized on flagellum cross-sections as electron-dense granules found between the membrane and the axoneme (Absalon et al., 2008). We examined multiple cross-sections of non-induced RNAi mutants. Particles showed a very specific location being found almost exclusively close to axoneme doublets 3-4 (Fig. 1A, 1B and 1F) and 7-8 (Fig. 1A, 1E), as previously reported (Absalon et al., 2008). In non-induced control *IFT88*$^{RNAi}$ cells, more than half of the flagellum cross-sections showed an IFT particle (n=224)(Fig. 1I). After two days of RNAi induction, this value dropped to less then 30% of sections (n=222)(Fig. 1C, 1D, I). In the case of *IFT140*$^{RNAi}$, 65% of the cross-sections through flagella in control cells presented IFT particles (n=177)(Fig. 1J). After two days of induction, barely 11% of the sections contained a single IFT particle (n=261). In contrast, close to 60%

of them were characterized by the presence of a large amount of electron-dense material (termed "pluri-density") that could correspond to IFT material (Fig. 1E, 1F, 1J). These results suggest that in the absence of IFT88, the number of IFT particles is reduced in the old flagellum whereas in *IFT140*$^{RNAi}$ cells, excessive material is visible.

**The distribution of IFT172 is altered in the old flagellum of IFT-A and IFT-B mutants**

To firmly correlate the modification in abundance of the electron dense structures with IFT, an ImmunoFluorescence Assay (IFA) was performed on methanol-fixed trypanosomes, using double labelling with MAb25, a monoclonal antibody that recognizes a protein found all along the axoneme (Pradel et al., 2006) and with a monoclonal antibody raised against IFT172, a classic IFT marker (Absalon et al., 2008; Blisnick et al., 2014). MAb25 produced staining along the whole length of the flagellum in both mature flagella (white arrows) and flagella undergoing construction (yellow arrows, Fig. 2A, 2C). The anti-IFT172 gave punctuate staining along the length of the flagellum and also lit up its base in non-induced *IFT88*$^{RNAi}$ and *IFT140*$^{RNAi}$ cells (Fig. 2A, 2C). In *IFT88*$^{RNAi}$ induced for 2 days, the majority of cells failed to assemble a new flagellum as revealed by little or no MAb25 signal (yellow arrowhead). Cells that retained the old flagellum only showed an IFT172 signal at the basal body area and very little, if any, signal along the axoneme (Fig. 2B). This result is consistent with the reduced number of IFT trains detected by transmission electron microscopy.

A very different result was obtained when *IFT140*$^{RNAi}$ cells were stained with the same antibodies (Fig. 2D). As expected, induced cells constructed only a short axoneme (short line as MAb25 signal)(yellow arrowhead in Fig. 2D) that accumulated IFT172 in agreement with the retrograde transport defect (Absalon et al., 2008). In contrast to *IFT88*$^{RNAi}$, a strikingly increased signal for IFT172 was observed along the length of the old flagellum (white arrowheads), especially at the distal region (circles, Fig. 2D). This is coherent with the

excessive number of visible IFT trains observed by transmission electron microscopy (Fig. 1G, 1H). We conclude that in the absence of anterograde transport, entry of IFT proteins in the old flagellum is restricted whereas in the absence of retrograde transport, IFT-B complex proteins accumulate in the persisting flagellum, presumably because of failure in train recycling.

**IFT trafficking is absent or arrested in flagella of IFT-A and IFT-B mutants**

IFT is a dynamic process with IFT particles travelling rapidly in both directions inside the flagellum. To monitor IFT in the old flagellum of *IFT88*$^{RNAi}$ and *IFT140*$^{RNAi}$ cells, they were nucleofected with a plasmid allowing expression of YFP::IFT81 (another component of IFT-B complex) from its endogenous locus (Bhogaraju et al., 2013). Western blot analysis confirmed the expression of YFP::IFT81 at the expected size of 113 kDa. Its total amount is not modified upon IFT88 or IFT140 knockdown (Supplementary material Fig. S1). Observation of live cells in non-induced *IFT88*$^{RNAi}$ and *IFT140*$^{RNAi}$ cultures revealed classic IFT trafficking in both new and old flagella. In both cell lines, YFP::IFT81 was concentrated at the flagellar base (Fig. 3A, star) and moved rapidly in both anterograde and retrograde directions in the flagellum (Supplementary movies 1, 3). The movement of IFT trains can be followed on still images (coloured arrowheads on Fig. 3A). Kymograph analysis was performed (example is shown on the last panel on Fig. 3A) to determine the speed and the frequency of anterograde trains. In the case of *IFT88*$^{RNAi}$ speed was 2.27 ± 0.72 µm/s and train frequency was 0.9/s (n=271). For *IFT140*$^{RNAi}$ cells, it was 2.66 ± 0.89 and 0.79/s (n=233). These values are within the usual range for IFT in trypanosomes (Bhogaraju et al., 2013; Blisnick et al., 2014; Buisson et al., 2013; Huet et al., 2014). In contrast, observation of live *IFT88*$^{RNAi}$ trypanosomes induced for two days showed a dramatic reduction in trafficking of IFT trains inside the flagellum (Fig. 3B) (Supplementary movie 2). IFT trafficking was not

visible, neither on videos nor on kymographs (n=28). In induced live *IFT140*$^{RNAi}$ cells, a bright YFP signal was present along the length of the flagellum especially in the distal region whereas the pool of IFT material at the basal body area was drastically reduced (Fig. 3B). Two different types of profiles can be described, with two thirds of the cells (n=16) showing abundant YFP::IFT81 signal along the whole flagellum length with a brighter signal at the distal tip whose intensity varied from one cell to another, with significant (Supplementary movie 4) to spectacular accumulations (Supplementary movie 5). In the remaining one third of cells, a continuous gradient of YFP::IFT81 from the distal to the proximal end of flagellum was observed (white brace, Fig. 3C, Supplementary movie 6). No IFT movement could be detected. These results formally show that IFT88 is essential for the entry of other IFT-B proteins whereas IFT140 is required for the return of IFT particles in already assembled flagella. They also demonstrate that IFT proteins undergo turnover in the mature flagellum, in contrast to what was initially thought (Kohl et al., 2003). This turnover is relatively slow as it takes hours to be detected, explaining it had been missed in photobleaching experiments that were focused on short acquisition period since the IFT cycle in the flagellum takes ~20 seconds (Buisson et al., 2013).

**Absence of IFT trafficking in the *IFT140*$^{RNAi}$ mutant**

Typical movement of IFT trains could not be identified in induced *IFT140*$^{RNAi}$ cells. However, traffic could still take place but be hidden by the intense fluorescent signal. To address this, Fluorescence Recovery After Photobleaching (FRAP) experiments were performed in *IFT140*$^{RNAi}$ cells expressing endogenously tagged YFP::IFT81. Cells were induced and a region of interest in the middle of the flagellum was selected for photobleaching. Only cells with a long flagellum were used to make sure this one indeed corresponded to an old flagellum. The fluorescence recovery was evaluated by continuously recording videos of live

cells for 45 sec and by kymograph analysis. Two different situations were observed. In 41% (n=15) of the videos, the photo-bleached region remained dark and exhibited no detectable recovery, with the fluorescent signal of the region of interest remaining at the background level. Typical IFT trafficking was clearly absent from both video images (Supplementary movie 7) and from analysis of the kymograph (data not shown). In the other videos, the photo-bleached region showed very weak recovery ranging from 2 to 9% of the initial signal (after 30 seconds, Fig. 3D & Supplementary movie 8). Kymograph analysis failed to detect typical IFT trafficking, even after enhancing brightness and contrast (Fig. 3D, last panel). However, a weak progressive return of fluorescence was detected in the periphery of the region of interest (indicated by yellow arrows on the kymograph, Fig. 3D), more suggestive of a diffusion-like process. These experiments confirm that IFT proteins present in the old flagellum of induced *IFT140*$^{RNAi}$ cells are indeed arrested and do not undergo IFT.

We conclude that in the absence of *IFT88* or *IFT140*, the typical IFT train trafficking along the old flagellum is lost. The silencing of IFT88 reveals that IFT trains cannot enter in the old flagellum whereas the silencing of IFT140 demonstrates an accumulation of IFT particles along the length of the flagellum in agreement with a default in train recycling. In both situations, flagella do not display active IFT. This allows addressing the biological significance of IFT trafficking in the mature flagellum.

**IFT is not necessary for the maintenance of flagellum length**

In the green algae *Chlamydomonas*, IFT trafficking is essential for the maintenance of flagellum length (Kozminski et al., 1995). In the absence of IFT, the axoneme disassembles progressively from its distal end. The average length of the flagellum appears reduced in trypanosome IFT RNAi mutants (Absalon et al., 2008; Absalon et al., 2007; Kohl et al., 2003). However, the situation is complex because trypanosomes maintain their flagellum

during the whole cell cycle. It is therefore of prime importance to discriminate the consequences of IFT RNAi silencing on construction and maintenance. We therefore examined the cell cycle and the length of the new and the old flagellum during the course of RNAi induction in *IFT88*$^{RNAi}$ cells and *IFT140*$^{RNAi}$ cells. We stained the axoneme with the MAb25 antibody and used DAPI to visualize nuclear and kinetoplast DNA (n>100). At the onset of the cell cycle, control trypanosomes possess a single nucleus (N) and a single mitochondrion whose genetic material is concentrated in an organelle named kinetoplast (K) that is physically linked to the basal body (Robinson and Gull, 1991). The progression of trypanosomes in the cell cycle can be followed by DNA staining as individuals with one kinetoplast and one nucleus (1K1N) are in the G1/S phase, those with two kinetoplasts and one nucleus (2K1N) are in G2/M and cells with two kinetoplasts and two nuclei (2K2N) are about to divide (Sherwin and Gull, 1989a)(see cartoons at Fig. 4A). Flagellum elongation (the growing flagellum is shown in yellow on all cartoons) starts immediately after basal body maturation and continues at a constant rate of 3-4 µm/hour throughout the rest of the cell cycle (Bastin et al., 1999).

Trypanosome cultures are not synchronized and cells in all phases of the cell cycle are present. For each cell line, we measured the length of the old and the new flagellum in non-induced cells and at an early induction time when IFT is aborted in the old flagellum (24h for *IFT88*$^{RNAi}$ and 48h for *IFT140*$^{RNAi}$). In non-induced 1K1N cells, the length of the old flagellum measured using the MAb25 staining was on average 15 µm for *IFT88*$^{RNAi}$ cells (Fig. 4B) and 18 µm for *IFT140*$^{RNAi}$ cells (Fig. 4F). This is a bit shorter compared with wild-type cells (19.5 µm) and is probably explained by RNAi leakiness (Absalon et al., 2007). At the 2K1N stage, the new flagellum can be at different stages of elongation resulting in a large heterogeneity in length as shown by the high dispersion (open red dots, Fig. 4C & G). This dispersion is due to the heterogeneity of this cell cycle stage where the flagellum elongates

from 1-2 to 15 µm (Sherwin and Gull, 1989a; Subota et al., 2014). The length of the old flagellum (closed red dots) was similar to cells with one flagellum (Fig. 4C, 4G). The 2K2N stage is a shorter phase preceding cytokinesis where the length of the new flagellum (open red dots) reaches about 80% of that of the old flagellum (Fig. 4D, 4H)(Robinson et al., 1995; Subota et al., 2014). The length of the old flagellum (closed red dots) was similar to what was observed for the two preceding stages of the cell cycle (Fig. 4D, 4H). One day after initiation of RNAi in the *IFT88*$^{RNAi}$ strain, construction of the new flagellum was impeded as revealed in 2K1N and 2K2N cells (Fig. 4C, 4D, open blue dots), in agreement with the essential role of IFT in flagellum construction (Kohl et al., 2003). In contrast, the length of the old flagellum (closed blue dots) was unchanged despite the fact that IFT was absent in these flagella (Fig. 4C, D). These results are summarised in the cartoons presented at Fig. 4E. IFT arrest emerges more slowly in *IFT140*$^{RNAi}$ cells and consequences were examined after two days of induction. It revealed interesting data with a mixture of 2 populations of 1K1N cells with different flagellum lengths. About half of the cells exhibited the same length as non-induced controls whereas the other half displayed much shorter flagella (< 5µm) (Fig. 4F, blue dots). Examination of 2K1N and 2K2N stages (Fig. 4G, 4H, closed blue dots) showed that these shorter cells are the daughters that inherited a flagellum that was constructed too short due to inhibition of retrograde IFT (Absalon et al., 2008) (Fig. 4G, 4H, open blue dots). The other half inherited the flagellum that was assembled prior to RNAi inhibition and these showed no reduction in length despite the fact that IFT is arrested (see cartoons at Fig. 4I).

These data confirm that IFT is essential for the construction of the new flagellum as expected but reveal that IFT is dispensable for maintenance of flagellum length. Indeed, the length of the mature flagellum is not reduced in the absence of IFT trafficking in both mutant cell lines. Since IFT trafficking requires energy, this raises the question of the role of IFT in the old flagellum. One possible explanation for the persistence of this machinery could be the

involvement of IFT in the turnover or the maintenance of flagellar components. To address this question, the fate of different categories of proteins was investigated: (1) skeletal proteins composing the axoneme and the PFR and (2) non-structural proteins.

**IFT is not necessary for the maintenance of skeletal flagellar components but is required for flagellar beating**

Flagella are complex organelles made of hundreds of proteins with variable structure, function and localisation (Broadhead et al., 2006; Oberholzer et al., 2011; Pazour et al., 2005; Subota et al., 2014). To determine the role of IFT trafficking in the maintenance of structural proteins within the old flagellum, we used either endogenous tagging of several typical axoneme or PFR markers or IFA with available antibodies in both *IFT88*$^{RNAi}$ cells and *IFT140*$^{RNAi}$ cells. First, the hydin axonemal central pair protein (Dawe et al., 2007; Lechtreck and Witman, 2007) was tagged with GFP, revealing presence all along the flagellum but also in the cell body as revealed by IFA with an anti-GFP (Supplementary material, Fig. S2) or by live video-microscopy (not shown). After RNAi induction, cells that had retained the old flagellum were still positive for hydin with no detectible modification of signal intensity in both cell lines (Supplementary material Fig. S2). A similar result was obtained when using a polyclonal antibody against the intermediate dynein chain (DNAI1) of the outer dynein arm (Duquesnoy et al., 2009): the flagellum signal was unchanged in the old flagella after two days of RNAi induction (data not shown).

We next turned our attention to the paraflagellar **rod** (PFR), a large axonemal structure found alongside the axoneme (Portman and Gull, 2010). One of its main components, the adenylate kinase B protein (AKB)(Pullen et al., 2004) was tagged with YFP and its presence and distribution was investigated in control and induced *IFT88*$^{RNAi}$ and *IFT140*$^{RNAi}$ cell lines (Supplementary material Fig. S3). In the non-induced situation, AKB was found in the

flagellum but only after its emergence from the cell body at the flagellar pocket level and double staining with the MAb25 axoneme marker confirmed a slightly off set positioning, in agreement with a PFR location (Supplementary material Fig. S3A, C). This pattern was not modified in the old flagella of induced samples (Supplementary material Fig. S3B, D). This was confirmed using a monoclonal antibody against PFR2, one of the major PFR proteins (Kohl et al., 1999) that showed the same fluorescence location and intensity in old flagella of induced samples (data not shown). These data indicate that the presence of structural axoneme and PFR components is not altered in the absence of IFT, in agreement with the apparently normal ultrastructure observed during the TEM analysis (Fig. 1). Therefore, we conclude that IFT is not necessary for the maintenance of these constituents after construction.

These results raise the question of the role of IFT in flagellum motility. Trypanosomes grow in suspension and swim actively in liquid medium (Heddergott et al., 2012). The movement of *IFT140*$^{RNAi}$ cells was quantified in non-induced control conditions and after 3 days of RNAi induction. Non-induced cells exhibited an average speed of 9.8 ± 2.8 µm/s (n=380)(Supplementary material Fig. S3E), in the expected range for procyclic trypanosomes in culture (Brasseur et al., 2013). Microscope observation revealed a striking reduction in motility that was confirmed by tracking analysis with an average speed at 2.8 ± 1.7 µm/s (n=987, p value < 0.0001) (Supplementary material Fig. S3F). Barely 1% of the cells displayed the control speed of 9 µm/s. At this stage, the population is composed of a mixture of trypanosomes that inherited either the flagellum that was assembled before RNAi or the short flagellum that was constructed after RNAi was initiated (Kohl et al., 2003). To discriminate the contribution of each population, immunofluorescence was carried out with the MAb25 axonemal marker. It revealed that ~50% of the induced cells still possessed a flagellum longer than 10 µm (n=125). Since cell tracking revealed that 99% of induced *IFT140*$^{RNAi}$ trypanosomes fail to show wild-type motility movement, these data demonstrate

that flagellar beating is significantly reduced in the absence of active IFT. As seen above, this is not due to visible structural defects in peripheral doublet organisation, dynein arms or central pair structure (Fig. 1). This motility phenotype could possibly be explained by discrete structural perturbations (dynein regulatory complex, radial spokes) or by modification of non-structural elements.

**IFT is required for the correct distribution of non-skeletal flagellar components**

The motility phenotype suggests that other flagellar components could be altered in the absence of IFT. Proteomics studies revealed a large number of flagellar proteins that are not strongly associated to the axoneme or the PFR (Oberholzer et al., 2011; Subota et al., 2014). The distribution of three such proteins was investigated. First, the protein kinase A regulatory subunit (PKAR) has been shown to localise to the flagellum matrix and to contribute to flagellum motility (Oberholzer et al., 2011). Endogenous tagging has been used to determine the presence and location of PKAR. In non-induced *IFT88*$^{RNAi}$ and *IFT140*$^{RNAi}$ cells, the protein is located probably to the PFR, as shown by the slightly off set signal compared to the MAb25 axoneme marker (Fig. 5A, 5C). After 2 days of RNAi induction, the signal was decreased in the old flagella of *IFT88*$^{RNAi}$ cells, a phenomenon accompanied by increased signal in the cytoplasm (Fig. 5B). In *IFT140*$^{RNAi}$ cells, the signal for YFP::PKAR in the old flagellum by IFA using anti-GFP antibodies remained unchanged, but additional cytoplasmic signal was observed after induction (Fig. 5D). These results suggest that IFT could be involved in the distribution of PKAR between the cytoplasm and the flagellum.

We next investigated the location of KIF9B protein, a kinesin molecular motor involved in the assembly of the PFR that is present along the axoneme and at the base of both old and new flagella (Demonchy et al., 2009). *IFT88*$^{RNAi}$ and *IFT140*$^{RNAi}$ cells were transfected to express a GFP::KIF9B fusion protein from its endogenous locus. Live cell

analysis revealed the presence of GFP::KIF9B at the flagellum base (circles on figures) and along the flagellum in both cell lines as expected (94% of cells, n=78) (Fig. 6A, 6C). Surprisingly, KIF9B was found concentrated at the distal tip of the old flagellum in the absence of IFT in both *IFT88*$^{RNAi}$ and *IFT140*$^{RNAi}$ cells (59% of cell, n=164)(arrowheads, Fig. 6B, 6D). The signal appeared as a nicely focused spot at the far end of the axoneme and was confirmed by IFA analysis with an anti-GFP (not shown). We conclude that the correct distribution of KIF9B at the base of the flagellum depends on IFT in mature flagella.

FLAM8 is a protein concentrated at the distal tip of the axoneme whose amount increases during flagellum construction and after cell division (Subota et al., 2014). A rabbit anti-FLAM8 antibody confirmed the distal tip localisation in the mature flagellum of control non-induced *IFT88*$^{RNAi}$ and *IFT140*$^{RNAi}$ cells (Fig. 7A, 7C). A different picture was obtained 24 hours after triggering RNAi: the staining at the tip was less intense and had the tendency to stretch in the proximal direction and multiple discrete spots appeared along the flagellum (arrowheads, Fig. 7B, 7C). One-dimensional projection of the flagellum based on the MAb25 marker confirmed the modified distribution pattern (Fig. 7, right panels). These results were reproduced with the anti-GFP antibody in *IFT88*$^{RNAi}$ and *IFT140*$^{RNAi}$ cells expressing YFP::FLAM8. The distal tip signal was reduced and shifted along the axoneme after 24 hours of induction (Supplementary material Fig. S4). We conclude that FLAM8 requires IFT activity to be maintained at the distal tip of the flagellum after assembly. Overall, these results demonstrate that IFT is not necessary for flagellum length maintenance but is required for the correct distribution of several non-structural proteins.

## Discussion

### IFT is not required for the maintenance of flagellum length

Knockdown of any individual *IFT* gene by inducible RNAi inhibits the construction of the new flagellum but the old flagellum persists during the course of RNAi induction (Kohl et al., 2003). We show here by a combination of TEM, IFA and video-microscopy that IFT is absent or arrested in the old flagellum (Fig. 8). This is explained if IFT proteins are slowly exchanged between the flagellar and the cytoplasmic compartment. In the case of anterograde mutants, a reduced import of IFT trains would not be sufficient to compensate those that exit, leading to a progressive depletion of IFT. For retrograde mutants, a progressive imbalance would emerge between trains that get in and trains that can be recycled, leading to excessive IFT material that cannot traffic anymore.

This loss of IFT activity in mature flagella is not accompanied by flagellum shortening (Fig. 8). Although a reduction of the average flagellum length is observed in trypanosome populations where RNAi has been induced, it is actually explained by the emergence of daughter cells that assembled a new flagellum that was too short. Cells that inherited the long old flagellum remain present but their proportion goes down progressively as they are diluted by daughter cells with a shorter flagellum.

To our knowledge, this paper is the first report of a situation where IFT is active in growing and mature flagella but is essential only for construction and not for maintenance of length. This could be explained if the flagellum does not undergo tubulin turnover, presumably because it is never disassembled (see below). Three other situations had been encountered so far in the literature regarding the presence and involvement of IFT in flagellum formation and maintenance. First, IFT is active in growing and mature flagella and is essential for construction and maintenance of length. This has formally been proven only in

*Chlamydomonas* but often considered as the norm. This makes sense if the organelle undergoes tubulin turnover at its distal end as encountered in *Chlamydomonas* (Marshall and Rosenbaum, 2001) and in *C. elegans* (Hao et al., 2011b). Second, IFT is active and essential only for flagellum construction, but becomes absent once the organelle has matured. This has been reported recently for the flagellum of mouse spermatozoa. IFT proteins are highly abundant during early stages of flagellum construction but are not detected in mature spermatozoa (San Agustin et al., 2015) and inhibition of IFT following absence of the KIF3A motor has severe consequences on flagellum formation (Lehti et al., 2013). This situation is by no means universal for all spermatozoa: for example two subunits of the heterotrimeric IFT kinesin II are well present in the flagellum of mature spermatozoa in sea urchin and sand dollar (Henson et al., 1997). Third, IFT is absent and obviously not required for flagellum construction when it takes place in the cytoplasm as reported for *Plasmodium* (Briggs et al., 2004; Sinden et al., 1976) and *Drosophila* (Han et al., 2003; Sarpal et al., 2003). These multiple situations further highlight the need to use different model organisms to study the breath of diversity in cilia and flagella (Morga and Bastin, 2013).

The unique situation reported here for trypanosomes could be explained by closer examination of the biology of the flagellum in this organism. In *Chlamydomonas* and *C. elegans*, IFT is required to bring tubulin to compensate the continuous turnover that takes places at the distal end of mature flagella (Craft et al., 2015; Hao et al., 2011b; Marshall and Rosenbaum, 2001). Two pieces of evidence indicate that there is little or no turnover in the skeletal elements of the mature flagellum of *Trypanosoma brucei.* First, tyrosinated tubulin, a marker of recently assembled tubulin, is only encountered at the tip of the new flagellum where immuno-gold staining or IFA displayed a clear gradient from tip to base but virtually no signal in the old flagellum (Sherwin and Gull, 1989b; Sherwin et al., 1987). This however cannot be investigated directly since tagged tubulin is not incorporated in the trypanosome

flagellum (Bastin et al., 1996; Sheriff et al., 2014). Second, inducible expression of an epitope-tagged PFR2 protein, a major component of the paraflagellar rod (PFR, a lattice-like structure associated to the axoneme) (Portman and Gull, 2010) revealed strong incorporation at the distal region of the new flagellum with only a discrete incorporation all along the old flagellum without any polarity (Bastin et al., 1999). This could well explain the different consequences of the absence of IFT in new and old flagella. When the new flagellum is assembled, tubulin and other flagellar proteins require IFT to be transported to the distal tip; hence IFT inhibition blocks flagellum formation. In the old flagellum, tubulin does not need to be replaced and therefore the loss of IFT does not result in flagellum shortening. This absence of shortening could be due to the sophisticated architecture of the trypanosome flagellum that contains a PFR physically connected to the axoneme and that is attached along most of the length of the cell body via another cytoskeletal structure called the flagellum attachment zone (Sunter and Gull, 2016). Accordingly, when trypanosomes produce developmental stages with a shorter flagellum length, this is always achieved by mean of an asymmetric division with the construction of a shorter new flagellum and not by shortening an existing flagellum (Ooi and Bastin, 2013; Rotureau et al., 2011; Sharma et al., 2008).

**IFT and the maintenance of flagellar components**

If IFT remains active in trypanosome flagella after construction, it is likely to fulfil other functions than assembly. One that springs to mind is the maintenance of flagellum components. TEM images show that the structure of the axoneme and of the associated PFR appears normal in the old flagellum of both induced *IFT88*$^{RNAi}$ and *IF140*$^{RNAi}$ cells, what is confirmed at the molecular level by the unmodified distribution of hydin, AKB or PFR1/2. Similar results were obtained in *Chlamydomonas* using metabolic labelling where most axoneme proteins show limited turnover once the flagellum has reached its final length,

although the actual contribution of IFT to this process could not formally be demonstrated (Song and Dentler, 2001). Investigation of a temperature-sensitive mutant for the IFT dynein heavy chain in this same organism revealed a 2- and 4-fold reduction in anterograde and retrograde IFT frequency, respectively but flagella maintained their length for about one day (Engel et al., 2012), in contrast to the *fla10* mutant where IFT is arrested and flagella are resorbed in 5 hours. 2D-DIGE comparative analysis of the composition of such flagella with controls revealed expected accumulation of several IFT proteins but also perturbations in the amounts of some membrane and matrix proteins, indicating likely functions for IFT in the control of their distribution in mature flagella (Engel et al., 2012).

However, the loss of flagellum beating in the absence of IFT indicates that these flagella are modified. We could identify modifications of the distribution of 3 non-structural proteins. The regulatory subunit of protein kinase A (PKAR) that is normally located in the matrix of the flagellum (Oberholzer et al., 2011) is drastically reduced in the flagellum whereas its concentration in the cytoplasm increases. This is reminiscent of the *Chlamydomonas* aurora-like kinase (CALK) that translocates from the cell body to the flagellum during gamete activation (Pan and Snell, 2000). CALK is resolved as two bands on SDS-PAGE both requiring the activity of the FLA10 kinesin II subunit either for exclusion from the flagellum or for efficient translocation respectively (Pan and Snell, 2003). Here, we propose that the PKAR shuttles between the cytoplasm and the flagellum in a process that is IFT-dependent. The cytoplasmic and flagellar compartments are separated with a diffusion barrier at the transition zone. This gate would restrict the entry of cytoplasmic molecules on the basis of their size (Kee et al., 2012) and/or shape (Breslow et al., 2013). The PKAR protein (57kDa) could be too large to enter by diffusion and would require energy to cross the gate. Preliminary FRAP analysis showed that flagellar YFP::PKAR diffuses within the flagellum without displaying typical IFT movement (our unpublished data). This suggests that

IFT could contribute to the concentration of PKAR in the flagellum perhaps via a transient association to cross the barrier between the cytoplasm and the flagellar compartment, followed by release and free diffusion inside the flagellum. This can be compared with some membrane ciliary proteins in mammalian cells (Ye et al., 2013) or even some structural components such as DRC4 in *Chlamydomonas* (Wren et al., 2013). In the absence of IFT, the PKAR is still produced in the cytoplasm but it cannot be transported efficiently in the flagellum, hence resulting in an inversion of the flagellum-to-cytoplasm signal ratio.

FLAM8 is a large protein found at the distal tip of the axoneme whose amount increases during flagellum construction, reaching about half of the concentration found in the mature flagellum at the time of cell division (Subota et al., 2014). We propose that FLAM8 is an IFT cargo that uses anterograde transport to reach the tip where it remains apparently stationary. After cell division, IFT is still active and more FLAM8 can be transported until a plateau is reached when the flagellum becomes mature. In the absence of IFT, FLAM8 proteins present in the old flagellum relocate towards the base, perhaps by diffusion following its concentration gradient (Fig. 8). In a normal situation, anterograde IFT would return these proteins to the distal tip, hence contributing to both constitution and maintenance of the FLAM8 distal location. Such a principle could be applied to other distal tip proteins (Liu et al., 2010; Saada et al., 2014; Woodward et al., 1995) or IFT-independent mechanisms could also exist as recently shown for the localisation of EB1 at the end of flagellar microtubules in *Chlamydomonas* (Harris et al., 2016). The motor action of IFT could hence define a micro-domain at the distal end of the flagellum. This could be significant knowing that trypanosomes swim with the flagellum forward and that they use the flagellum to attach to the epithelium of the salivary glands during infection in the tsetse fly (Tetley and Vickerman, 1985). Signalling molecules could also be concentrated depending on IFT (Eguether et al., 2014).

KIF9B is present along the axoneme and located at the base of both old and new flagella. In the absence of KIF9B, trypanosomes assemble an apparently normal axoneme but the construction of the PFR is defective: large "blocks" of PFR materials alternate with regions where only the axoneme is present (Demonchy et al., 2009). It was suggested that the motor activity of KIF9B somehow contributes to the transport of PFR proteins during construction of the structure. We propose that KIF9B walks towards the plus end of flagellum microtubules using its motor activity, perhaps transporting PFR components or other elements necessary for PFR assembly. Once KIF9B reaches the tip of the flagellum, it cannot return by itself and needs retrograde IFT to be recycled to the base. KIF9B would therefore be an IFT cargo but only for retrograde transport. In both mutants where retrograde transport is abolished (directly in *IFT140*$^{RNAi}$ and because of lack of trains in first place in the *IFT88*$^{RNAi}$ strain), KIF9B would still be able to reach the tip of the flagellum because this would rely solely on its own activity but would not be able to return, resulting in the tip fluorescent signal observed (Fig. 8). This process emerges relatively late (2-3 days after RNAi induction), possibly either because of slow displacement of KIF9B or in case if only a proportion of KIF9B was motile. This is compatible with the absence of GFP::KIF9B movement in short video acquisitions (Demonchy et al., 2009).

Overall, these data demonstrate that IFT is necessary to create and maintain micro-domains within the flagellum by concentrating or removing specific proteins. IFT activity and association to various cargoes therefore could allow the generation of molecular diversity inside cilia by concentrating (or excluding) sensors, structural elements or other motors. This is relevant for multi-cellular organisms that produce several types of cilia but also in protists that assemble different types of flagella either in the same cell (Dawson and House, 2010) or in different life cycle stages (Gluenz et al., 2010; Rotureau et al., 2012). In addition to protein distribution, IFT could to the transport of other molecules. The lipid composition of flagella

appears very different from the rest of the cell membrane (Serricchio et al., 2015) and the fact that IFT trains are in tightly contact with the flagellar membrane (Absalon et al., 2008; Kozminski et al., 1993) is intriguing. In conclusion, IFT appears a key player in the composition and maintenance of cilia and flagella, in addition to its well-characterised role in construction. Investigating these functions in different species promises to reveal novel exciting features.

## Materials and methods

### Trypanosome cell lines and cultures

Cell lines used for this work were derivatives of *T. brucei* strain 427 and cultured in SDM79 medium supplemented with hemin and 10% foetal calf serum (Brun and Schonenberger, 1979). The *IFT88*$^{RNAi}$ (Kohl et al., 2003) and *IFT140*$^{RNAi}$ (Absalon et al., 2008) cell lines have been described previously. These cell lines express complementary single-stranded RNA corresponding to a fragment of the *IFT88* or the *IFT140* gene from two tetracycline-inducible T7 promoters facing each other in the pZJM vector (Wang et al., 2000) integrated in the rDNA locus of 29-13 cells that express the T7 RNA polymerase and the tetracycline repressor (Wirtz et al., 1999). Addition of tetracycline (1µg/mL) to the medium induces expression of sense and anti-sense RNA strands that can anneal to form double-stranded RNA (dsRNA) and trigger RNAi.

### Plasmid construction and transformation in trypanosomes

Genecust Europe (Luxembourg) synthesised the insert *PKAR* (GeneDB number Tb927.11.4610), *RSP9* (Tb927.8.810) and *AKB* (Tb927.10.830) that were then cloned in the p2675 plasmid allowing YFP tagging at the N-terminal end of proteins of interest (Kelly et al., 2007). The gene fragment *PKAR* (1-476 nucleotides), *RSP9* (1-496 nucleotides) and *AKB* (1-476 nucleotides) were digested with HindIII and ApaI respectively and cloned into the corresponding sites of the p2675 vector. Each p2675 construct was linearized with a specific enzyme allowing recombination within the *PKAR* (SgrdI), *RSP9* (BbsI) or *AKB* (NsiI) gene. The eGFP::Hydin fusion contains 1-1,200 bp of the *hydin* gene in frame downstream of the *eGFP* gene in the vector pPCPFReGFP (Adhiambo et al., 2009). In this vector, the fusion gene is flanked by *PFR1* and *PFR2* intergenic sequences. The vector was linearized by EcoRI

and integrated in the hydin endogenous locus, resulting in a reconstructed complete eGFP::Hydin fusion. Plasmids p2675YFPIFT81 (Bhogaraju et al., 2013), pPCPFReGFPKIF9B (Demonchy et al., 2009) and p3329FLAM8 (Subota et al., 2014) have been described previously.

*IFT88*$^{RNAi}$ and *IFT140*$^{RNAi}$ cell lines were transfected with the above plasmids by Nucleofector technology (Lonza, Italy) as described (Burkard et al., 2007). Transfectants were grown in media with the appropriate antibiotic concentration and clonal populations were obtained by limiting dilution. Cell lines were characterized either by phase contrast or direct fluorescence observation (eGFP or YFP). Cell culture growth was monitored daily with an automatic Muse cell analyzer (Merck Millipore, Paris).

**Immunofluorescence (IFA) and live cell imaging**

Cultured parasites were washed twice in SDM79 medium without serum and spread directly onto poly-L-lysine coated slides. The slides were air-dried for 10 min, fixed in methanol at −20°C for 5 min and rehydrated for 20 min in PBS (Sherwin et al., 1987). For immunodetection, slides were incubated with primary antibodies diluted in phosphate-buffered saline (PBS) with 0.1% Bovine Serum Albumin (BSA) for 1 hour at room temperature or at 37°C in a humid chamber. Slides were washed in PBS and appropriate subclass-specific secondary antibodies coupled to Alexa 488 or Alexa 594 (Invitrogen), and Cy3 or Cy5 (Jackson ImmunoResearch, West Grove, PA) were added using a 1:400 dilution in PBS with 0.1% BSA. After 45 min incubation, slides were washed in PBS then 4′,6-diamidino-2-phenyl-indole (DAPI) (2 µg/µl) staining of the nucleus and the kinetoplast was performed. Slides were mounted using ProLong antifade reagent (Invitrogen). Samples were observed with a DMI4000 Leica microscope, and images were acquired with a Horca 03G (Hamamatsu, Hamamatsu City, Japan) camera. In the case of RNAi mutants, all IFA signals

were normalized using the signal obtained in non-induced controls as a reference.

The monoclonal antibody MAb25 (IgG2a)(Pradel et al., 2006), which specifically recognizes the axoneme protein TbSAXO1 (Dacheux et al., 2012), was used as flagellum marker. The IFT complex B IFT172 protein was recognized using anti-IFT172 mouse monoclonal antibody diluted 1:200 (Blisnick et al., 2014). GFP was observed directly or upon fixation by immunofluorescence using a 1:200 dilution of a rabbit anti-GFP antibody (Invitrogen). FLAM8 was detected using a rabbit polyclonal serum (1:1,000 dilution) that was kindly provided by Paul McKean (University of Lancaster, UK).

GFP/YFP visualization on live trypanosomes was performed as described (Buisson et al., 2013). IFT videos were acquired using a Zeiss inverted microscope (Axiovert 200; Jena, Germany) equipped with an oil immersion objective (magnification 100× with numerical aperture 1.4) and a spinning disk confocal head (CSU22; Yokogawa, Tokyo, Japan). Images were acquired using Volocity software with an electron-multiplying charge-coupled device camera (C-9100; Hamamatsu) operating in streaming mode. A sample of parasites (6 to $8.10^6$ cells/mL) was taken directly from the culture and trapped between slide and coverslip. The samples were kept at ambient temperature and used no longer than 30 min. Images were analyzed using ImageJ (National Institutes of Health, Bethesda, MD). NeuronJ plugin was used to measure the flagellum length. Kymograph analysis (Buisson et al., 2013; Chenouard et al., 2010) and cell tracking for motility (Brasseur et al., 2013) were performed exactly as described.

**Fluorescent Recovery After Photobleaching (FRAP) Analysis**

The expression of YFP::IFT81 in the *IFT140*$^{RNAi}$ background was first observed directly with a DMI4000 Leica microscope using an EL6000 (Leica) or LED light source (Spectra X, Lumencor) for excitation to confirm correct protein expression and localization. For FRAP

analysis, a spinning disk confocal head (UltraView Vox, Perkin Elmer) was used. Images were acquired using Volocity software with an EMCCD camera (ImagEM X2, Hamamatsu) operating in streaming mode. A parasite sample from induced *IFT140*$^{RNAi}$ expressing YFP::IFT81 was taken directly from the culture grown at 6 to 8.10$^{6}$ cells/mL and trapped between slide and coverslip. The samples were kept at room temperature and a region of interest was defined within the flagellum. Images were recorded continuously for 5 sec before bleaching and then recovery was monitored for 45 sec by continuously recording videos with a 100 ms exposure.

**Transmission and scanning electron microscopy (TEM)**

For transmission electron microscopy (TEM), cells were fixed directly in medium during 10 min at room temperature in 2.5% glutaraldehyde (Glutaraldehyde 25% stock solution, EM Grade, Electron Microscopy Sciences). Centrifugation was carried out at 4°C for 5 min at 580 *g*. The supernatant was discarded and the pellet was fixed in 2.5% glutaraldehyde and 4% PFA (paraformaldehyde 32% stock solution, EM Grade, Electron Microscopy Sciences) in 0.1 M cacodylate buffer (pH 7.2) and contrasted with OsO4 (2%) (Osmium tetroxide 4% Aqueous solution, Electron Microscopy Sciences) in cacodylate buffer. After serial dehydration with ethanol solutions, samples were embedded in Agar 100 (Agar Scientific, Ltd., United Kingdom) and left to polymerize at 60°C for 2 days. Ultrathin sections (50–70 nm thick) were collected on Formvar-carbon-coated nickel grids using a Leica EM UC6 ultra-microtome and stained with uranyl acetate (2%, w/v) (Uranyl Acetate dehydrate, Electron Microscopy Sciences) and lead citrate (80 mM, home made buffer). Observations were made on a Tecnai BioTWIN 120 cryo electron microscope (FEI) and images were captured with a MegaView II camera (Arecont Vision, France) and processed with AnalySIS and Adobe Photoshop CS4 (San Jose, CA).

**Western blot**

Cells were washed in PBS and pellets were boiled in Laemmli loading buffer before SDS-PAGE separation, loading 20 µg of total cell protein per lane. Proteins were transferred to polyvinylidene fluoride membranes overnight at 4°C under low voltage (25V). Membranes were blocked with 5% reconstituted skimmed milk in PBS-Tween 0.1% (PBST) and incubated with primary antibodies diluted in 1% reconstituted skim milk and PBST. A mixture of two anti-GFP monoclonal antibodies (Roche, Life Science) was used to detect YFP and eGFP (1:200 dilution) whereas the anti-BIP was diluted 1:1000 (Bangs et al., 1993) and served as loading control. Three membrane washes were performed with PBST for 5 min. Species-specific secondary antibodies coupled to horseradish peroxidase (GE Healthcare) were diluted 1:20,000 in PBST containing 1% milk and incubated for 1 hr. Detection was carried out by using an enhanced chemiluminescence assay and the imaging system Pxi (Ozyme, France).

## Acknowledgements

We thank Brice Rotureau for help in quantitative analysis of cell motility. We acknowledge Derrick Robinson and Paul McKean for generous gifts of antibodies, and Raphaël Demonchy for preliminary observations of the KIF9B phenotype. We thank Jean-Yves Tinevez (Imagopole) and Gérard Pehau-Arnaudet (Ultrapole) for training and valuable advises for light and electron microscopy, respectively.

### Competing interests

The authors declare no competing or financial interests.

### Author contributions

C.F., S.B. & P.B. conceived and designed the experiments; C.F. and S.B. performed the experiments; L.K. contributed reagents, materials and commented on the manuscript; C.F. and P.B. wrote the manuscript.

### Funding

C.F. is supported by fellowships from French National Ministry for Research and Technology (doctoral school CDV515) and from La Fondation pour la Recherche Médicale (FDT20150532023). This work was funded by ANR grants (11-BSV8-016 and 14-CE35-0009-01) and by La Fondation pour la Recherche Médicale (Equipe FRM DEQ20150734356).

## References


**Absalon, S., Blisnick, T., Kohl, L., Toutirais, G., Dore, G., Julkowska, D., Tavenet, A. and Bastin, P.** (2008). Intraflagellar Transport and Functional Analysis of Genes Required for Flagellum Formation in Trypanosomes. *Mol Biol Cell* **19**, 929-944.

**Absalon, S., Kohl, L., Branche, C., Blisnick, T., Toutirais, G., Rusconi, F., Cosson, J., Bonhivers, M., Robinson, D. and Bastin, P.** (2007). Basal Body Positioning Is Controlled by Flagellum Formation in Trypanosoma brucei. *PLoS ONE* **2**, e437.

**Adhiambo, C., Blisnick, T., Toutirais, G., Delannoy, E. and Bastin, P.** (2009). A novel function for the atypical small G protein Rab-like 5 in the assembly of the trypanosome flagellum. *J Cell Sci* **122**, 834-41.

**Bangs, J. D., Uyetake, L., Brickman, M. J., Balber, A. E. and Boothroyd, J. C.** (1993). Molecular cloning and cellular localization of a BiP homologue in Trypanosoma brucei. Divergent ER retention signals in a lower eukaryote. *J Cell Sci* **105 ( Pt 4)**, 1101-13.

**Bastin, P., Bagherzadeh, Z., Matthews, K. R. and Gull, K.** (1996). A novel epitope tag system to study protein targeting and organelle biogenesis in Trypanosoma brucei. *Mol Biochem Parasitol* **77**, 235-9.

**Bastin, P., Ellis, K., Kohl, L. and Gull, K.** (2000). Flagellum ontogeny in trypanosomes studied via an inherited and regulated RNA interference system. *J Cell Sci* **113 ( Pt 18)**, 3321-8.

**Bastin, P., MacRae, T. H., Francis, S. B., Matthews, K. R. and Gull, K.** (1999). Flagellar morphogenesis: protein targeting and assembly in the paraflagellar rod of trypanosomes. *Mol Cell Biol* **19**, 8191-200.

**Bhogaraju, S., Cajanek, L., Fort, C., Blisnick, T., Weber, K., Taschner, M., Mizuno, N., Lamla, S., Bastin, P., Nigg, E. A. et al.** (2013). Molecular basis of tubulin transport within the cilium by IFT74 and IFT81. *Science* **341**, 1009-12.

**Blisnick, T., Buisson, J., Absalon, S., Marie, A., Cayet, N. and Bastin, P.** (2014). The intraflagellar transport dynein complex of trypanosomes is made of a heterodimer of dynein heavy chains and of light and intermediate chains of distinct functions. *Mol Biol Cell* **25**, 2620-33.

**Brasseur, A., Rotureau, B., Vermeersch, M., Blisnick, T., Salmon, D., Bastin, P., Pays, E., Vanhamme, L. and Perez-Morga, D.** (2013). Trypanosoma brucei FKBP12 differentially controls motility and cytokinesis in procyclic and bloodstream forms. *Eukaryot Cell* **12**, 168-81.

**Breslow, D. K., Koslover, E. F., Seydel, F., Spakowitz, A. J. and Nachury, M. V.** (2013). An in vitro assay for entry into cilia reveals unique properties of the soluble diffusion barrier. *J Cell Biol* **203**, 129-47.

**Briggs, L. J., Davidge, J. A., Wickstead, B., Ginger, M. L. and Gull, K.** (2004). More than one way to build a flagellum: comparative genomics of parasitic protozoa. *Curr Biol* **14**, R611-2.

**Broadhead, R., Dawe, H. R., Farr, H., Griffiths, S., Hart, S. R., Portman, N., Shaw, M. K., Ginger, M. L., Gaskell, S. J., McKean, P. G. et al.** (2006). Flagellar motility is required for the viability of the bloodstream trypanosome. *Nature* **440**, 224-7.

**Brown, J. M., Fine, N. A., Pandiyan, G., Thazhath, R. and Gaertig, J.** (2003). Hypoxia regulates assembly of cilia in suppressors of Tetrahymena lacking an intraflagellar transport subunit gene. *Mol Biol Cell* **14**, 3192-207.

**Brown, J. M., Marsala, C., Kosoy, R. and Gaertig, J.** (1999). Kinesin-II is preferentially targeted to assembling cilia and is required for ciliogenesis and normal cytokinesis in Tetrahymena. *Mol Biol Cell* **10**, 3081-96.

**Brun, R. and Schonenberger.** (1979). Cultivation and in vitro cloning or procyclic culture forms of Trypanosoma brucei in a semi-defined medium. Short communication. *Acta Trop* **36**, 289-92.

**Buisson, J., Chenouard, N., Lagache, T., Blisnick, T., Olivo-Marin, J. C. and Bastin, P.** (2013). Intraflagellar transport proteins cycle between the flagellum and its base. *J Cell Sci* **126**, 327-38.

**Burkard, G., Fragoso, C. M. and Roditi, I.** (2007). Highly efficient stable transformation of bloodstream forms of Trypanosoma brucei. *Mol Biochem Parasitol* **153**, 220-3.

**Chenouard, N., Buisson, J., Bloch, I., Bastin, P. and Olivo-Marin, J. C.** (2010). Curvelet analysis of kymograph for tracking bi-directional particles in flurescence microscopy images. *International Conference on Image Processing*, in press.

**Cole, D. G., Diener, D. R., Himelblau, A. L., Beech, P. L., Fuster, J. C. and Rosenbaum, J. L.** (1998). Chlamydomonas kinesin-II-dependent intraflagellar transport (IFT): IFT particles contain proteins required for ciliary assembly in Caenorhabditis elegans sensory neurons. *J Cell Biol* **141**, 993-1008.

**Craft, J. M., Harris, J. A., Hyman, S., Kner, P. and Lechtreck, K. F.** (2015). Tubulin transport by IFT is upregulated during ciliary growth by a cilium-autonomous mechanism. *J Cell Biol* **208**, 223-37.

**Dacheux, D., Landrein, N., Thonnus, M., Gilbert, G., Sahin, A., Wodrich, H., Robinson, D. R. and Bonhivers, M.** (2012). A MAP6-related protein is present in protozoa and is involved in flagellum motility. *PLoS ONE* **7**, e31344.

**Davidge, J. A., Chambers, E., Dickinson, H. A., Towers, K., Ginger, M. L., McKean, P. G. and Gull, K.** (2006). Trypanosome IFT mutants provide insight into the motor location for mobility of the flagella connector and flagellar membrane formation. *J Cell Sci* **119**, 3935-43.

**Dawe, H. R., Shaw, M. K., Farr, H. and Gull, K.** (2007). The hydrocephalus inducing gene product, Hydin, positions axonemal central pair microtubules. *BMC Biol* **5**, 33.

**Dawson, S. C. and House, S. A.** (2010). Life with eight flagella: flagellar assembly and division in Giardia. *Curr Opin Microbiol* **13**, 480-90.

**Deane, J. A., Cole, D. G., Seeley, E. S., Diener, D. R. and Rosenbaum, J. L.** (2001). Localization of intraflagellar transport protein IFT52 identifies basal body transitional fibers as the docking site for IFT particles. *Curr Biol* **11**, 1586-90.

**Demonchy, R., Blisnick, T., Deprez, C., Toutirais, G., Loussert, C., Marande, W., Grellier, P., Bastin, P. and Kohl, L.** (2009). Kinesin 9 family members perform separate functions in the trypanosome flagellum. *J Cell Biol* **187**, 615-22.

**Drummond, I. A.** (2012). Cilia functions in development. *Curr Opin Cell Biol* **24**, 24-30.

**Duquesnoy, P., Escudier, E., Vincensini, L., Freshour, J., Bridoux, A. M., Coste, A., Deschildre, A., de Blic, J., Legendre, M., Montantin, G. et al.** (2009). Loss-of-function mutations in the human ortholog of Chlamydomonas reinhardtii ODA7 disrupt dynein arm assembly and cause primary ciliary dyskinesia. *Am J Hum Genet* **85**, 890-6.

**Eguether, T., San Agustin, J. T., Keady, B. T., Jonassen, J. A., Liang, Y., Francis, R., Tobita, K., Johnson, C. A., Abdelhamed, Z. A., Lo, C. W. et al.** (2014). IFT27 links the BBSome to IFT for maintenance of the ciliary signaling compartment. *Dev Cell* **31**, 279-90.

**Engel, B. D., Ishikawa, H., Wemmer, K. A., Geimer, S., Wakabayashi, K., Hirono, M., Craige, B., Pazour, G. J., Witman, G. B., Kamiya, R. et al.** (2012). The role of retrograde intraflagellar transport in flagellar assembly, maintenance, and function. *J Cell Biol* **199**, 151-67.

**Franklin, J. B. and Ullu, E.** (2010). Biochemical analysis of PIFTC3, the Trypanosoma brucei orthologue of nematode DYF-13, reveals interactions with established and putative intraflagellar transport components. *Mol Microbiol* **78**, 173-86.

**Gluenz, E., Ginger, M. L. and McKean, P. G.** (2010). Flagellum assembly and function during the Leishmania life cycle. *Curr Opin Microbiol* **13**, 473-9.

**Han, Y. G., Kwok, B. H. and Kernan, M. J.** (2003). Intraflagellar transport is required in Drosophila to differentiate sensory cilia but not sperm. *Curr Biol* **13**, 1679-86.

**Hao, L., Efimenko, E., Swoboda, P. and Scholey, J. M.** (2011a). The retrograde IFT machinery of C. elegans cilia: two IFT dynein complexes? *PLoS ONE* **6**, e20995.

**Hao, L., Thein, M., Brust-Mascher, I., Civelekoglu-Scholey, G., Lu, Y., Acar, S., Prevo, B., Shaham, S. and Scholey, J. M.** (2011b). Intraflagellar transport delivers tubulin isotypes to sensory cilium middle and distal segments. *Nat Cell Biol* **13**, 790-8.

**Harris, J. A., Liu, Y., Yang, P., Kner, P. and Lechtreck, K. F.** (2016). Single-particle imaging reveals intraflagellar transport-independent transport and accumulation of EB1 in Chlamydomonas flagella. *Mol Biol Cell* **27**, 295-307.

**Haycraft, C. J., Swoboda, P., Taulman, P. D., Thomas, J. H. and Yoder, B. K.** (2001). The C. elegans homolog of the murine cystic kidney disease gene Tg737 functions in a ciliogenic pathway and is disrupted in osm-5 mutant worms. *Development* **128**, 1493-505.

**Heddergott, N., Kruger, T., Babu, S. B., Wei, A., Stellamanns, E., Uppaluri, S., Pfohl, T., Stark, H. and Engstler, M.** (2012). Trypanosome motion represents an adaptation to the crowded environment of the vertebrate bloodstream. *PLoS Pathog* **8**, e1003023.

**Henson, J. H., Cole, D. G., Roesener, C. D., Capuano, S., Mendola, R. J. and Scholey, J. M.** (1997). The heterotrimeric motor protein kinesin-II localizes to the midpiece and flagellum of sea urchin and sand dollar sperm. *Cell Motil Cytoskeleton* **38**, 29-37.

**Huang, B., Rifkin, M. R. and Luck, D. J.** (1977). Temperature-sensitive mutations affecting flagellar assembly and function in Chlamydomonas reinhardtii. *J Cell Biol* **72**, 67-85.

**Huet, D., Blisnick, T., Perrot, S. and Bastin, P.** (2014). The GTPase IFT27 is involved in both anterograde andretrograde intraflagellar transport. *eLife 2014;10.7554/eLife.02419*.

**Julkowska, D. and Bastin, P.** (2009). Tools for analysing intraflagellar transport in trypanosomes. *Meth Cell Biol* **93**, 59-80.

**Kee, H. L., Dishinger, J. F., Blasius, T. L., Liu, C. J., Margolis, B. and Verhey, K. J.** (2012). A size-exclusion permeability barrier and nucleoporins characterize a ciliary pore complex that regulates transport into cilia. *Nat Cell Biol* **14**, 431-7.

**Kelly, S., Reed, J., Kramer, S., Ellis, L., Webb, H., Sunter, J., Salje, J., Marinsek, N., Gull, K., Wickstead, B. et al.** (2007). Functional genomics in Trypanosoma brucei: a collection of vectors for the expression of tagged proteins from endogenous and ectopic gene loci. *Mol Biochem Parasitol* **154**, 103-9.

**Kohl, L., Robinson, D. and Bastin, P.** (2003). Novel roles for the flagellum in cell morphogenesis and cytokinesis of trypanosomes. *Embo J* **22**, 5336-46.

**Kohl, L., Sherwin, T. and Gull, K.** (1999). Assembly of the paraflagellar rod and the flagellum attachment zone complex during the Trypanosoma brucei cell cycle. *J Eukaryot Microbiol* **46**, 105-9.

**Kozminski, K. G., Beech, P. L. and Rosenbaum, J. L.** (1995). The *Chlamydomonas* kinesin-like protein FLA10 is involved in motility associated with the flagellar membrane. *J Cell Biol* **131**, 1517-27.

**Kozminski, K. G., Johnson, K. A., Forscher, P. and Rosenbaum, J. L.** (1993). A motility in the eukaryotic flagellum unrelated to flagellar beating. *Proc Natl Acad Sci U S A* **90**, 5519-23.

**Lechtreck, K. F. and Witman, G. B.** (2007). Chlamydomonas reinhardtii hydin is a central pair protein required for flagellar motility. *J Cell Biol* **176**, 473-82.

**Lee, E., Sivan-Loukianova, E., Eberl, D. F. and Kernan, M. J.** (2008). An IFT-A protein is required to delimit functionally distinct zones in mechanosensory cilia. *Curr Biol* **18**, 1899-906.

**Lehti, M. S., Kotaja, N. and Sironen, A.** (2013). KIF3A is essential for sperm tail formation and manchette function. *Mol Cell Endocrinol* **377**, 44-55.

**Liu, W., Apagyi, K., McLeavy, L. and Ersfeld, K.** (2010). Expression and cellular localisation of calpain-like proteins in Trypanosoma brucei. *Mol Biochem Parasitol* **169**, 20-6.

**Marshall, W. F. and Rosenbaum, J. L.** (2001). Intraflagellar transport balances continuous turnover of outer doublet microtubules: implications for flagellar length control. *J Cell Biol* **155**, 405-14.

**Morga, B. and Bastin, P.** (2013). Getting to the heart of intraflagellar transport using Trypanosoma and Chlamydomonas models: the strength is in their differences. *Cilia* **2**, 16.

**Nonaka, S., Tanaka, Y., Okada, Y., Takeda, S., Harada, A., Kanai, Y., Kido, M. and Hirokawa, N.** (1998). Randomization of left-right asymmetry due to loss of nodal cilia generating leftward flow of extraembryonic fluid in mice lacking KIF3B motor protein. *Cell* **95**, 829-37.

**Oberholzer, M., Langousis, G., Nguyen, H. T., Saada, E. A., Shimogawa, M. M., Jonsson, Z. O., Nguyen, S. M., Wohlschlegel, J. A. and Hill, K. L.** (2011). Independent analysis of the flagellum surface and matrix proteomes provides insight into flagellum signaling in mammalian-infectious Trypanosoma brucei. *Mol Cell Proteomics* **10**, M111 010538.

**Ooi, C. P. and Bastin, P.** (2013). More than meets the eye: understanding Trypanosoma brucei morphology in the tsetse. *Front Cell Infect Microbiol* **3**, 1-12.

**Orozco, J. T., Wedaman, K. P., Signor, D., Brown, H., Rose, L. and Scholey, J. M.** (1999). Movement of motor and cargo along cilia. *Nature* **398**, 674.

**Pan, J. and Snell, W. J.** (2000). Regulated targeting of a protein kinase into an intact flagellum. An aurora/Ipl1p-like protein kinase translocates from the cell body into the flagella during gamete activation in chlamydomonas. *J Biol Chem* **275**, 24106-14.

**Pan, J. and Snell, W. J.** (2003). Kinesin II and regulated intraflagellar transport of Chlamydomonas aurora protein kinase. *J Cell Sci* **116**, 2179-86.

**Pazour, G. J., Agrin, N., Leszyk, J. and Witman, G. B.** (2005). Proteomic analysis of a eukaryotic cilium. *J Cell Biol* **170**, 103-13.

**Pazour, G. J., Baker, S. A., Deane, J. A., Cole, D. G., Dickert, B. L., Rosenbaum, J. L., Witman, G. B. and Besharse, J. C.** (2002). The intraflagellar transport protein, IFT88, is essential for vertebrate photoreceptor assembly and maintenance. *J Cell Biol* **157**, 103-13.

**Pazour, G. J., Dickert, B. L., Vucica, Y., Seeley, E. S., Rosenbaum, J. L., Witman, G. B. and Cole, D. G.** (2000). *Chlamydomonas* IFT88 and Its Mouse Homologue, Polycystic Kidney Disease Gene Tg737, Are Required for Assembly of Cilia and Flagella. *J Cell Biol* **151**, 709-718.

**Pedersen, L. B., Geimer, S. and Rosenbaum, J. L.** (2006). Dissecting the molecular mechanisms of intraflagellar transport in chlamydomonas. *Curr Biol* **16**, 450-9.

**Pigino, G., Geimer, S., Lanzavecchia, S., Paccagnini, E., Cantele, F., Diener, D. R., Rosenbaum, J. L. and Lupetti, P.** (2009). Electron-tomographic analysis of intraflagellar transport particle trains in situ. *J Cell Biol* **187**, 135-48.

**Piperno, G. and Mead, K.** (1997). Transport of a novel complex in the cytoplasmic matrix of Chlamydomonas flagella. *Proc Natl Acad Sci U S A* **94**, 4457-62.

**Portman, N. and Gull, K.** (2010). The paraflagellar rod of kinetoplastid parasites: from structure to components and function. *Int J Parasitol* **40**, 135-48.

**Pradel, L. C., Bonhivers, M., Landrein, N. and Robinson, D. R.** (2006). NIMA-related kinase TbNRKC is involved in basal body separation in Trypanosoma brucei. *J Cell Sci* **119**, 1852-63.

**Pullen, T. J., Ginger, M. L., Gaskell, S. J. and Gull, K.** (2004). Protein targeting of an unusual, evolutionarily conserved adenylate kinase to a eukaryotic flagellum. *Mol Biol Cell* **15**, 3257-65.

**Robinson, D. R. and Gull, K.** (1991). Basal body movements as a mechanism for mitochondrial genome segregation in the trypanosome cell cycle. *Nature* **352**, 731-3.

**Robinson, D. R., Sherwin, T., Ploubidou, A., Byard, E. H. and Gull, K.** (1995). Microtubule polarity and dynamics in the control of organelle positioning, segregation, and cytokinesis in the trypanosome cell cycle. *J Cell Biol* **128**, 1163-72.

**Rotureau, B., Subota, I. and Bastin, P.** (2011). Molecular bases of cytoskeleton plasticity during the Trypanosoma brucei parasite cycle. *Cell Microbiol* **13**, 705-16.

**Rotureau, B., Subota, I., Buisson, J. and Bastin, P.** (2012). A new asymmetric division contributes to the continuous production of infective trypanosomes in the tsetse fly. *Development* **139**, 1842-50.

**Saada, E. A., Kabututu, Z. P., Lopez, M., Shimogawa, M. M., Langousis, G., Oberholzer, M., Riestra, A., Jonsson, Z. O., Wohlschlegel, J. A. and Hill, K. L.** (2014). Insect stage-specific receptor adenylate cyclases are localized to distinct subdomains of the Trypanosoma brucei Flagellar membrane. *Eukaryot Cell* **13**, 1064-76.

**San Agustin, J. T., Pazour, G. J. and Witman, G. B.** (2015). Intraflagellar transport is essential for mammalian spermiogenesis but is absent in mature sperm. *Mol Biol Cell* **26**, 4358-72.

**Sarpal, R., Todi, S. V., Sivan-Loukianova, E., Shirolikar, S., Subramanian, N., Raff, E. C., Erickson, J. W., Ray, K. and Eberl, D. F.** (2003). Drosophila KAP interacts with the kinesin II motor subunit KLP64D to assemble chordotonal sensory cilia, but not sperm tails. *Curr Biol* **13**, 1687-96.

**Serricchio, M., Schmid, A. W., Steinmann, M. E., Sigel, E., Rauch, M., Julkowska, D., Bonnefoy, S., Fort, C., Bastin, P. and Butikofer, P.** (2015). Flagellar membranes are rich in raft-forming phospholipids. *Biol Open* **4**, 1143-53.

**Sharma, R., Peacock, L., Gluenz, E., Gull, K., Gibson, W. and Carrington, M.** (2008). Asymmetric cell division as a route to reduction in cell length and change in cell morphology in trypanosomes. *Protist* **159**, 137-51.

**Sheriff, O., Lim, L. F. and He, C. Y.** (2014). Tracking the biogenesis and inheritance of subpellicular microtubule in Trypanosoma brucei with inducible YFP-alpha-tubulin. *Biomed Res Int* **2014**, 893272.

**Sherwin, T. and Gull, K.** (1989a). The cell division cycle of Trypanosoma brucei brucei: timing of event markers and cytoskeletal modulations. *Philos Trans R Soc Lond B Biol Sci* **323**, 573-88.

**Sherwin, T. and Gull, K.** (1989b). Visualization of detyrosination along single microtubules reveals novel mechanisms of assembly during cytoskeletal duplication in trypanosomes. *Cell* **57**, 211-21.

**Sherwin, T., Schneider, A., Sasse, R., Seebeck, T. and Gull, K.** (1987). Distinct localization and cell cycle dependence of COOH terminally tyrosinolated alpha-tubulin in the microtubules of Trypanosoma brucei brucei. *J Cell Biol* **104**, 439-46.

**Signor, D., Wedaman, K. P., Orozco, J. T., Dwyer, N. D., Bargmann, C. I., Rose, L. S. and Scholey, J. M.** (1999). Role of a class DHC1b dynein in retrograde transport of IFT motors and IFT raft particles along cilia, but not dendrites, in chemosensory neurons of living Caenorhabditis elegans. *J Cell Biol* **147**, 519-30.

**Sinden, R. E., Canning, E. U. and Spain, B.** (1976). Gametogenesis and fertilization in Plasmodium yoelii nigeriensis: a transmission electron microscope study. *Proc R Soc Lond B Biol Sci* **193**, 55-76.

**Song, L. and Dentler, W. L.** (2001). Flagellar protein dynamics in Chlamydomonas. *J Biol Chem* **276**, 29754-63.

**Subota, I., Julkowska, D., Vincensini, L., Reeg, N., Buisson, J., Blisnick, T., Huet, D., Perrot, S., Santi-Rocca, J., Duchateau, M. et al.** (2014). Proteomic analysis of intact flagella of procyclic Trypanosoma brucei cells identifies novel flagellar proteins with unique sub-localization and dynamics. *Mol Cell Proteomics* **13**, 1769-86.

**Sun, Z., Amsterdam, A., Pazour, G. J., Cole, D. G., Miller, M. S. and Hopkins, N.** (2004). A genetic screen in zebrafish identifies cilia genes as a principal cause of cystic kidney. *Development* **131**, 4085-93.

**Sunter, J. D. and Gull, K.** (2016). The Flagellum Attachment Zone: 'The Cellular Ruler' of Trypanosome Morphology. *Trends Parasitol*.

**Tetley, L. and Vickerman, K.** (1985). Differentiation in Trypanosoma brucei: host-parasite cell junctions and their persistence during acquisition of the variable antigen coat. *J Cell Sci* **74**, 1-19.

**Vincensini, L., Blisnick, T. and Bastin, P.** (2011). 1001 model organisms to study cilia and flagella. *Biol Cell* **103**, 109-30.

**Wang, Z., Morris, J. C., Drew, M. E. and Englund, P. T.** (2000). Inhibition of trypanosoma brucei gene expression by RNA interference using an integratable vector with opposing T7 promoters. *J Biol Chem* **275**, 40174-9.

**Wirtz, E., Leal, S., Ochatt, C. and Cross, G. A.** (1999). A tightly regulated inducible expression system for conditional gene knock-outs and dominant-negative genetics in Trypanosoma brucei. *Mol Biochem Parasitol* **99**, 89-101.

**Woodward, R., Carden, M. J. and Gull, K.** (1995). Immunological characterization of cytoskeletal proteins associated with the basal body, axoneme and flagellum attachment zone of Trypanosoma brucei. *Parasitology* **111 ( Pt 1)**, 77-85.

**Wren, K. N., Craft, J. M., Tritschler, D., Schauer, A., Patel, D. K., Smith, E. F., Porter, M. E., Kner, P. and Lechtreck, K. F.** (2013). A differential cargo-loading model of ciliary length regulation by IFT. *Curr Biol* **23**, 2463-71.

**Ye, F., Breslow, D. K., Koslover, E. F., Spakowitz, A. J., Nelson, W. J. and Nachury, M. V.** (2013). Single molecule imaging reveals a major role for diffusion in the exploration of ciliary space by signaling receptors. *Elife* **2**, e00654.

**Figures**

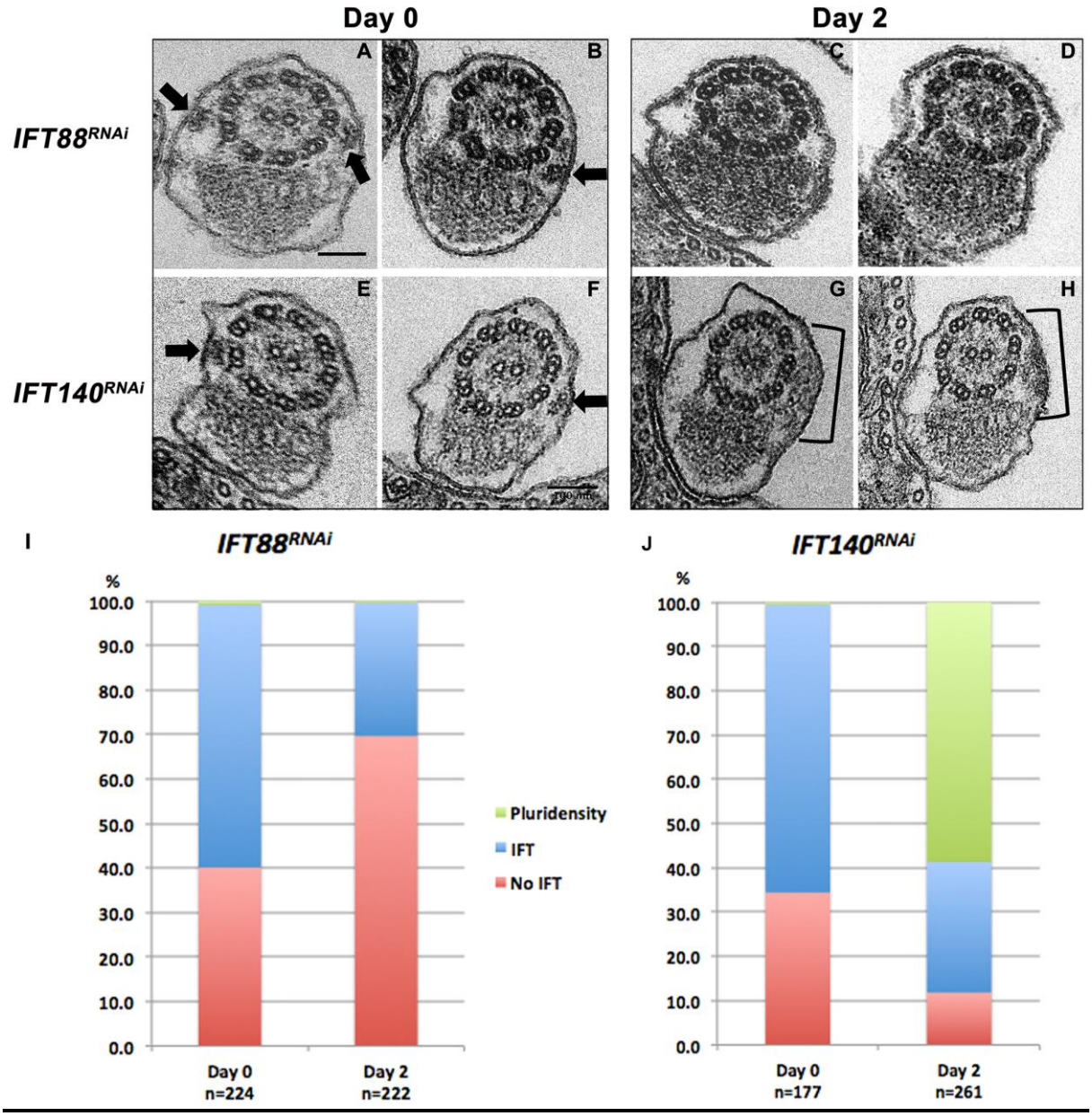


**Fig. 1**: Abundance of IFT particles in flagella of *IFT88*$^{RNAi}$ and *IFT140*$^{RNAi}$ cells. Cross-sections through the flagella of *IFT88*$^{RNAi}$ (A-D) or *IFT140*$^{RNAi}$ (E-H) cells. IFT particles are indicated with black arrows. (A-B and E-F) are non-induced cells whereas (C, D) and (G, H) correspond to cells after 2 days in RNAi conditions. IFT particles are frequently detected in

non-induced cells but are less commonly encountered in *IFT88*$^{RNAi}$ induced cells. In the absence of *IFT140*, excessively- large dense particles become frequent (indicated by bracket: G, H). Bar, 100 nm. (I, J) Percentage of IFT particles in cross-sections of *IFT88*$^{RNAi}$ (I) and *IFT140*$^{RNAi}$ (J) cells. In both graphs, the left bar indicates the percentage of sections without (red) or with (blue) an IFT particle, or with excessive material ("pluri-density", green) in non-induced cells. The right bar indicates the results obtained after 2 days of induction. Total number of sections (from 2 separate experiments) is indicated at the bottom of each graph.

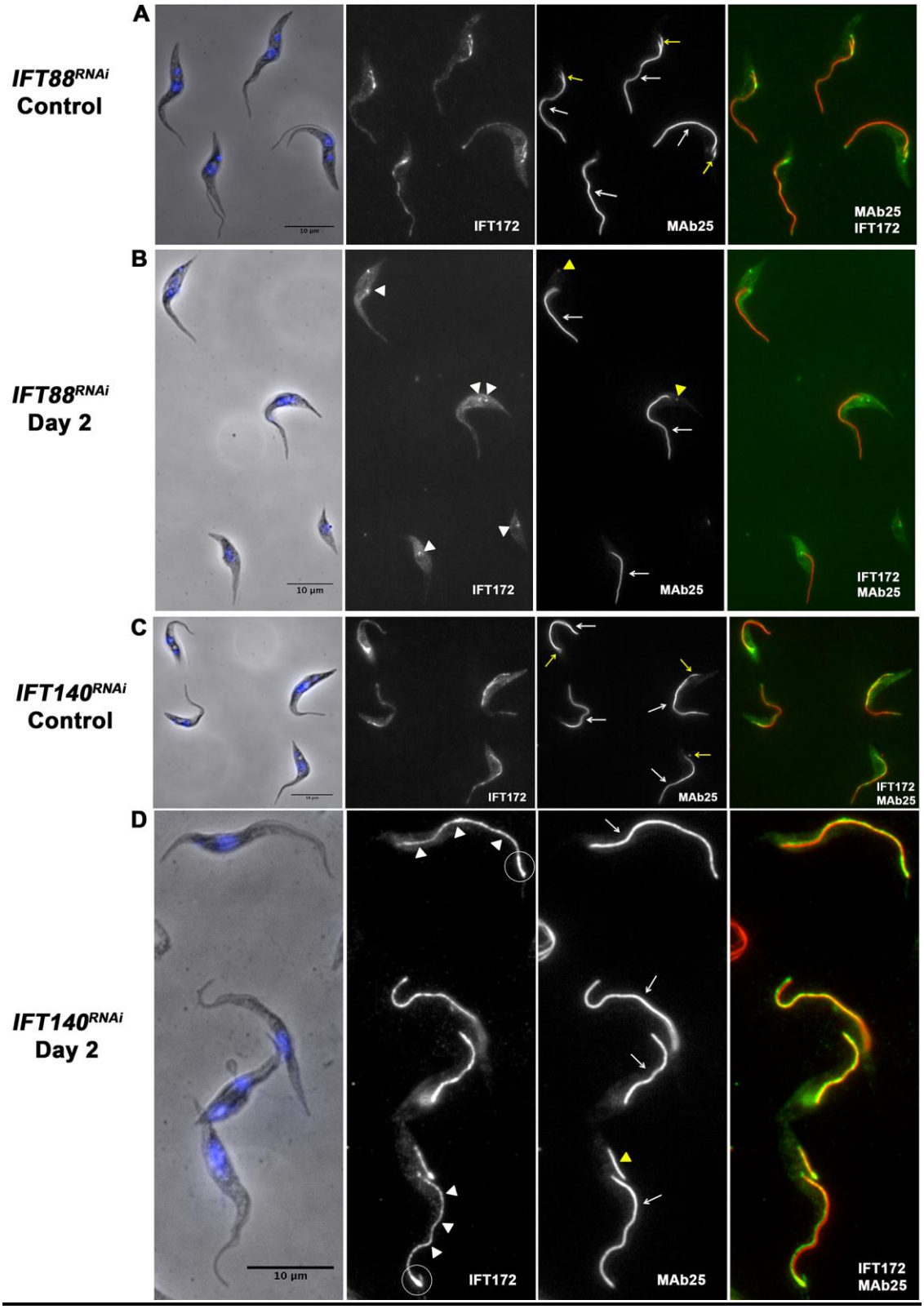

**Fig. 2**: Localization of IFT172 in trypanosome flagella. *IFT88*$^{RNAi}$ (A-B) and *IFT140*$^{RNAi}$ (C-D) cells have been fixed in methanol for 5 min and stained with a 1:100 dilution of the anti-IFT172 antibody (green), with a 1:10 dilution of the anti-axoneme MAb25 antibody (red) and with DAPI to reveal nuclear and kinetoplast DNA (blue). Fields of *IFT88*$^{RNAi}$ (A) and *IFT140*$^{RNAi}$ (C) non-induced cells. Yellow arrows indicate new flagella and white arrows point at old flagella. Induced cells for *IFT88*$^{RNAi}$ (B) or *IFT140*$^{RNAi}$ (D) displayed defects in flagellum construction. New flagella were absent in *IFT88*$^{RNAi}$ (yellow arrowheads) whereas they were short and dilated with an excessive amount of IFT172 protein in *IFT140*$^{RNAi}$ (yellow arrowhead). Notice the strongly reduced IFT172 signal in old flagella and the increased signal at the base (white arrowheads) in *IFT88*$^{RNAi}$ cells and the excessive signal in old flagella of *IFT140*$^{RNAi}$ cells (white arrowheads), especially at the distal tip (circles).

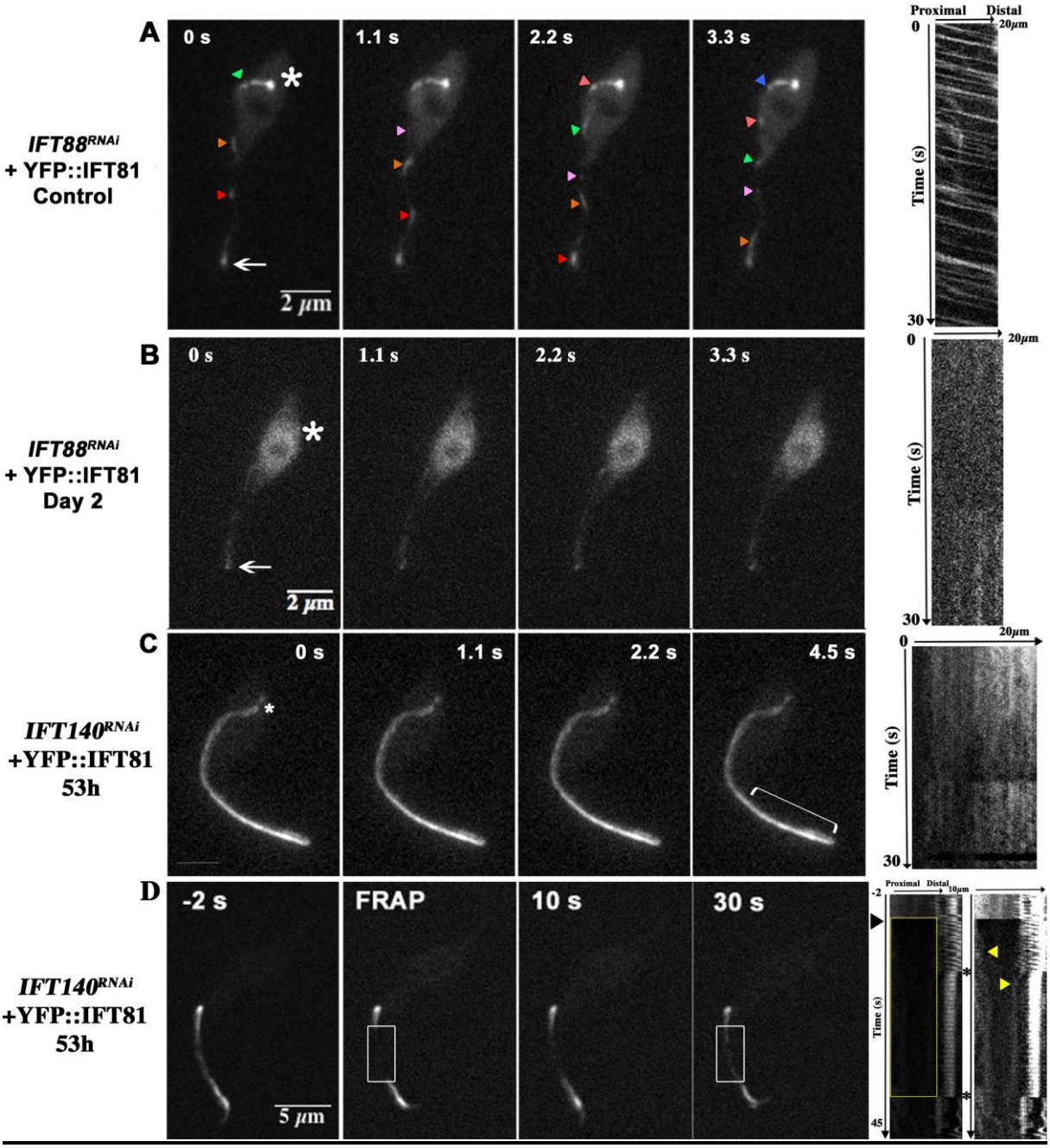


**Fig. 3**: Intraflagellar movement of YFP::IFT81 is lost in *IFT88*$^{RNAi}$ cells and arrested in *IFT140*$^{RNAi}$ cells. Still images are from movies of *IFT88*$^{RNAi}$ or *IFT140*$^{RNAi}$ cells expressing YFP::IFT81. (A) Anterograde intraflagellar movement of YFP::IFT81 in non-induced *IFT88*$^{RNAi}$ cells (Supplementary data movie 1). The coloured arrowheads indicate the

successive position of several anterograde trains on each image. Time is indicated on top of each image. The last panels show the kymograph analysis. On the first image, the white star indicates the position of the base of the flagellum and the white arrow marks the distal end of the flagellum. (B) After two days of induction, *IFT88*$^{RNAi}$ cells display weak YFP::IFT81 signal but no movement of IFT particles could be observed in the flagellum (movie 2). (C) In induced *IFT140*$^{RNAi}$ cells, IFT signal forms a continuous gradient along the length of the flagellum from the tip to the base indicated by a white brace on the last image (movie 4). (D) A bright fluorescent YFP::IFT81 signal is present along the length of the flagellum after 53h of induction in *IFT140*$^{RNAi}$ cells. A short portion of the flagellum (within the white box) was bleached with a brief laser pulse. The left image represents the fluorescence status before bleaching whereas the second one shows immediately after bleaching and the two last pictures of the series are extracted from the indicated time series acquisition. The time where bleaching took place is indicated by the black arrowhead. The stars indicate movements of the flagella, leading to a shift in signal position. The first image is the regular kymograph whereas the second one is the same where brightness and contrast were enhanced to facilitate visualisation of the minor recovery. **The striped pattern visible on the right-hand is due to the width of the region of interest that is slightly wider to take into account the movement of the flagellum.** After bleaching, low fluorescence gradually returns in the region of interest but does not display IFT-like movement. The yellow arrowheads indicate possible diffusion-like events coming from both ends of the bleached region. Bar, 2 µm.

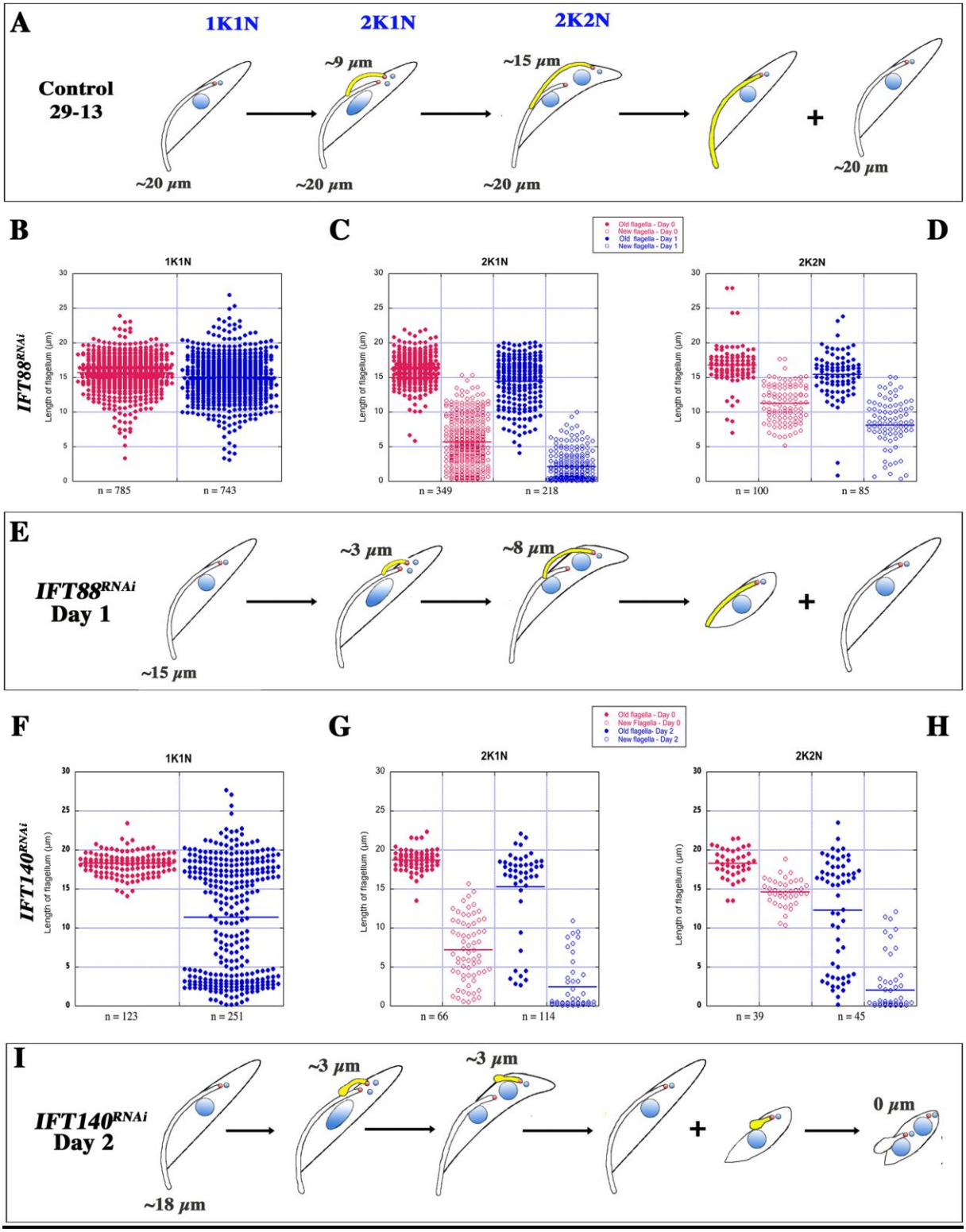

**Fig. 4**: Flagellum length evolution according to the cell cycle stage in wild-type, *IFT88*$^{RNAi}$ and *IFT140*$^{RNAi}$ cells. Non-induced (blue) or induced (red) cells were fixed in methanol and stained with the axoneme marker MAb25. (A) A cartoon to illustrate the cell cycle progression of a wild-type trypanosome. Old and new flagella are shown in white and in yellow, respectively whereas the basal body is in red and the nuclei and kinetoplasts are coloured in blue. The average length of old and new flagella at the various stages is indicated. The length of the flagellum was measured using the NeuronJ plugin in 1K1N cells (B, F), and the length of both the old (closed circles) and the new (open circles) flagellum was measured in bi-flagellated cells either at the 2K1N (C, G) or the 2K2N (D, H) stage. Number of measured flagella for each sample is indicated at the bottom of each graph. See text for details. Cartoons illustrating the cell cycle progression of *IFT88*$^{RNAi}$ cells (E) and *IFT140*$^{RNAi}$ cells (I) at the indicated time of induction are shown with the same colour code as above.

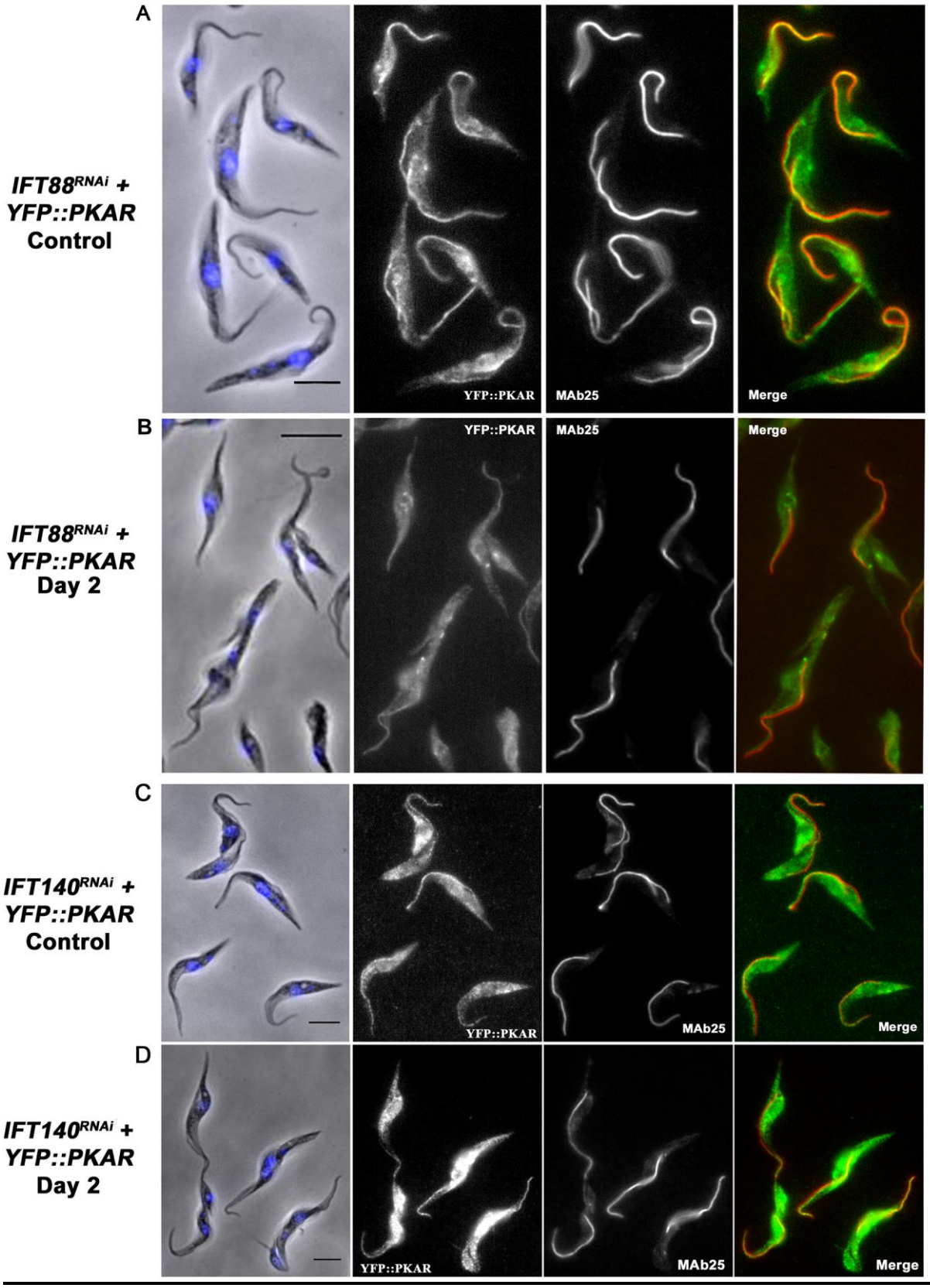

**Fig. 5**: Visualization of YFP::PKAR protein distribution in *IFT88*$^{RNAi}$ (A-B) and *IFT140*$^{RNAi}$ (C-D) cells. IFA was performed using the anti-GFP antibody (white and green in merge), the anti axoneme MAb25 antibody (white, red in merged panels) and counterstained with DAPI (blue) in the indicated cell lines and conditions. The fusion protein becomes more abundant in the cytoplasm in the induced conditions. Bar, 5 µm.

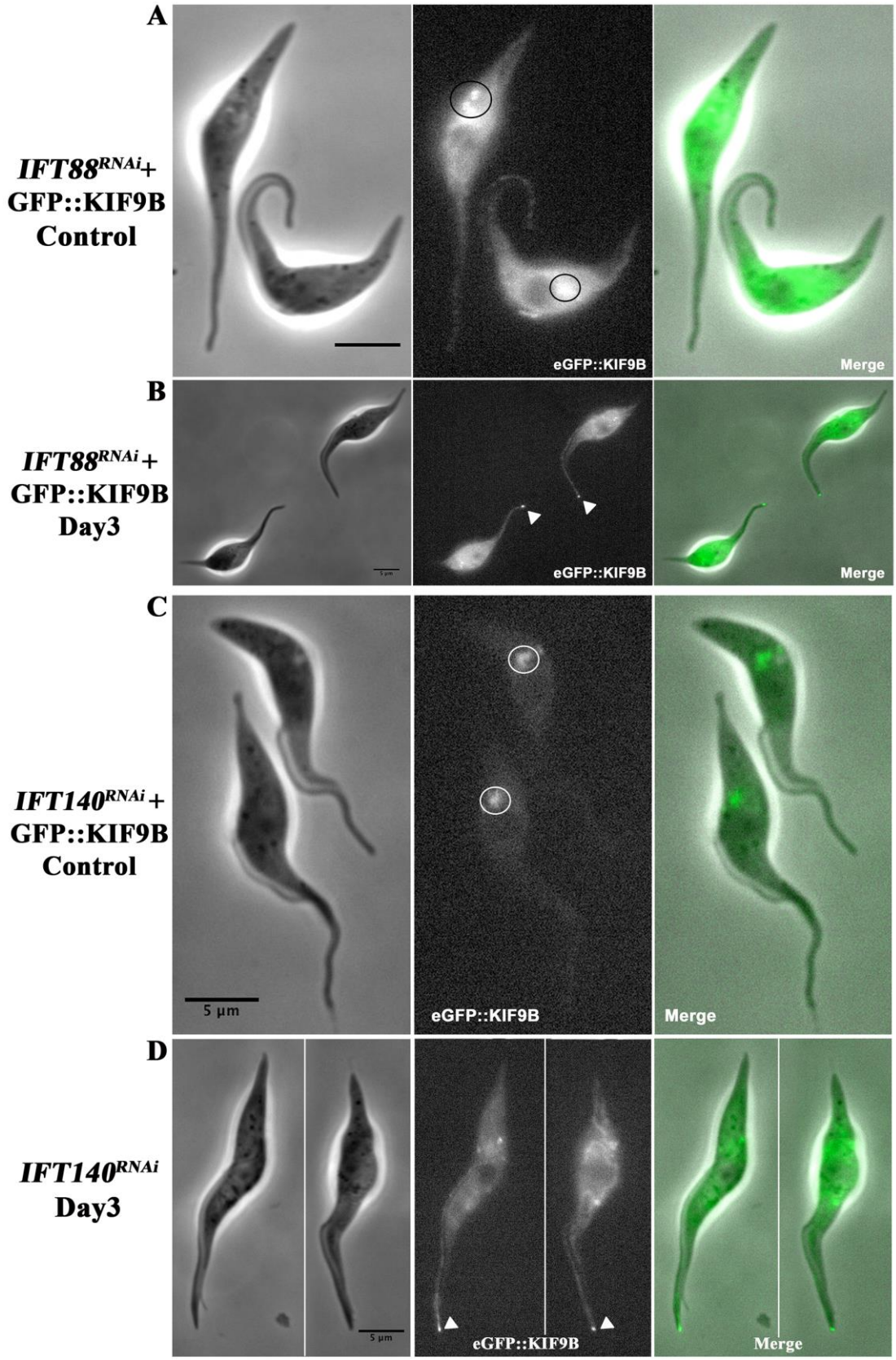

**Fig. 6:** Visualization of eGFP::KIF9B protein in live *IFT88*$^{RNAi}$ (A-B) and *IFT140*$^{RNAi}$ (C-D) cells. Images of cells expressing eGFP::KIF9B where circles indicate the base of the flagellum and white arrowheads the tip of flagellum. First series of images correspond to the phase contrast image, the second one shows the eGFP::KIB9B signal (white) and the third one shows the merged panels (GFP shown in green). Notice the presence of eGFP::KIF9B at the base of flagellum in control but at the tip (arrowheads) in induced conditions when IFT becomes inactive. Bar, 5 µm.

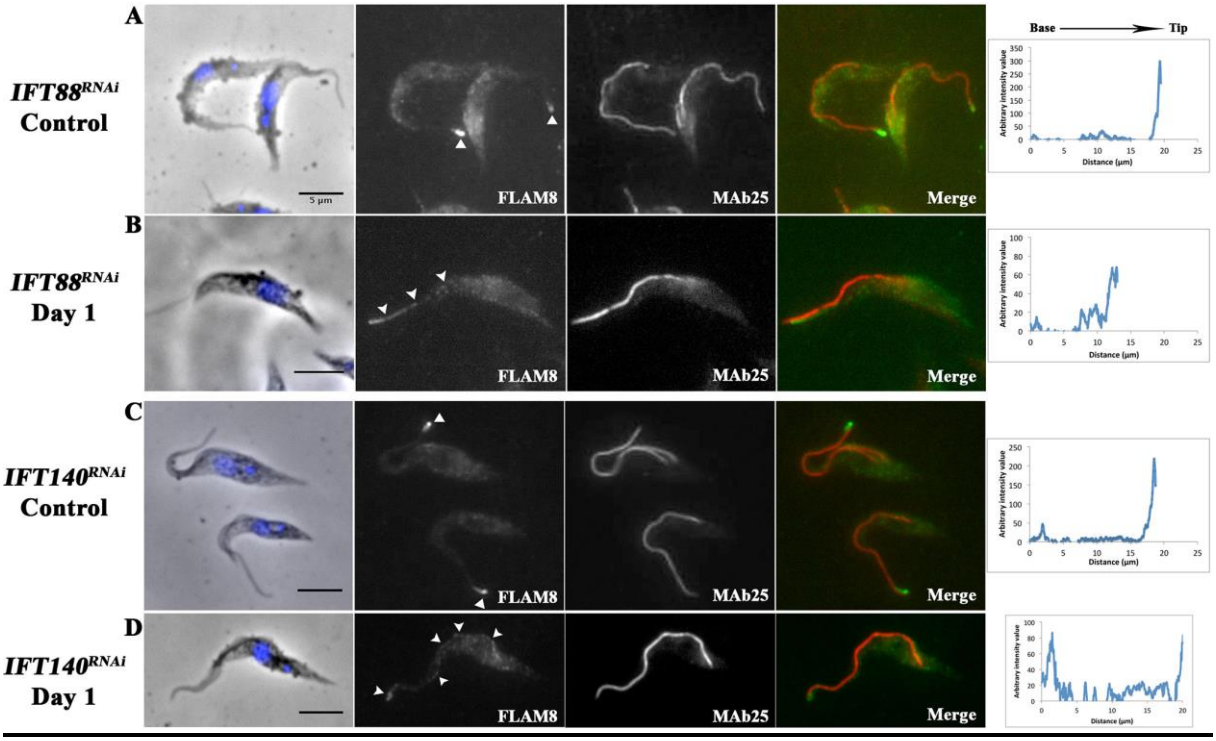


**Fig. 7**: Visualization of FLAM8::YFP protein in whole *IFT88*$^{RNAi}$ (A-B) and *IFT140*$^{RNAi}$ (C-D) cells. IFA was performed using an anti-GFP antibody (white and green in merge), the anti axoneme MAb25 antibody (white, red in merged panels) and counterstained with DAPI (blue) in the indicated cell lines and conditions. White arrowheads indicate the presence of YFP::FLAM8 protein at the tip of flagella (A, C) or along their length in induced *IFT88*$^{RNAi}$ and *IFT140*$^{RNAi}$ cells (B, D). Bar, 5 µm. Right, one-axis projections show the intensity of the signal along the length of the flagellum.

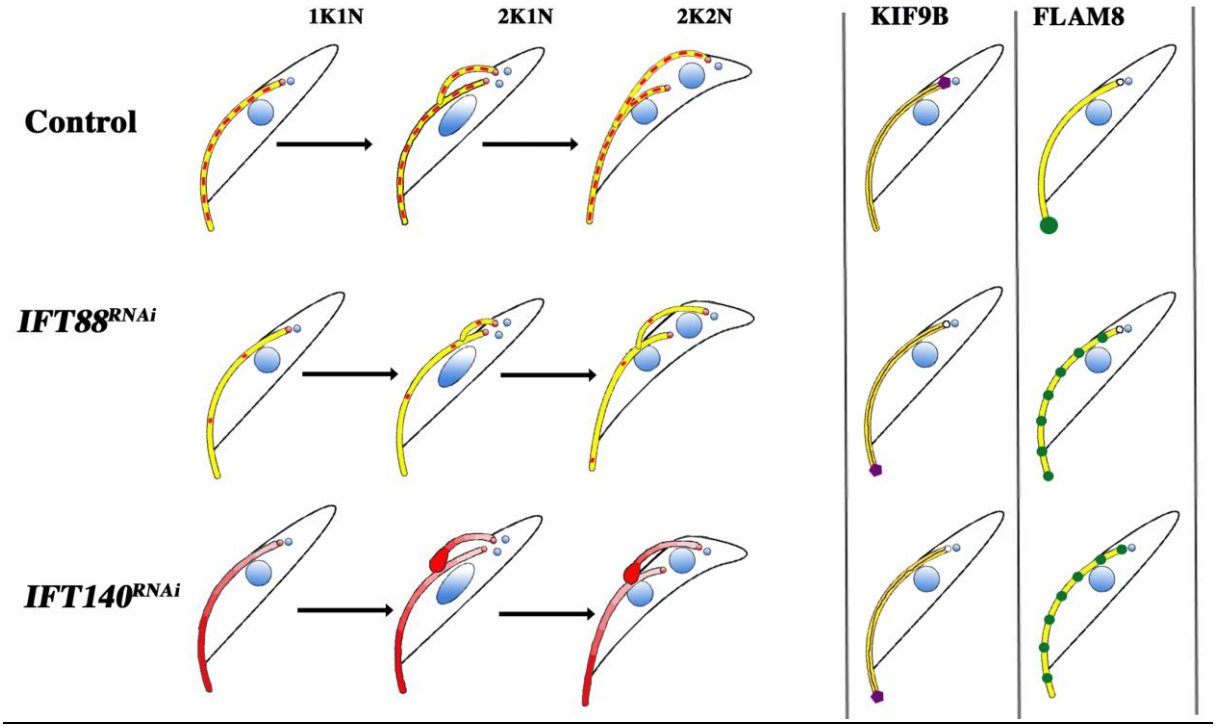


**Fig. 8.** Absence or arrest of IFT impacts differently on mature or growing flagella. On the left, the cell cycle of each cell line is indicated. IFT trains are shown in red whereas the nuclei and kinetoplasts are coloured in blue. In control situation, IFT is active in mature and growing flagellum. Upon RNAi silencing of IFT88, trains are getting less and less frequent and construction of the new flagellum is slowed down. However, the length of the old flagellum is not affected. Knockdown of IFT140 leads to failure in train recycling and accumulation of IFT material in both old and new flagella. This interferes with flagellum construction but not with maintenance of the length of the mature flagellum. On the right, the impact of absence or arrest of IFT in the mature flagellum on the distribution of KIF9B (violet) and FLAM8 (green) is shown. IFT trains have not been drawn on these panels for the sake of simplicity.

**Supplementary data**

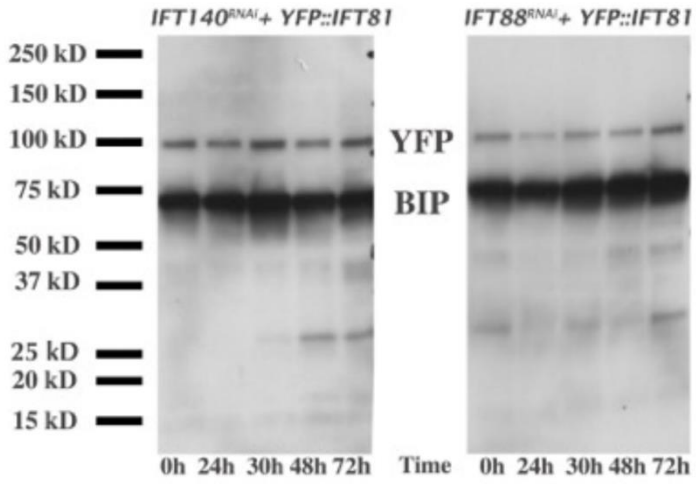


**Fig. S1:** Western blot showing expression levels of the YFP::IFT81 fusion protein in *IFT88*$^{RNAi}$ and *IFT140*$^{RNAi}$ cells. Proteins were separated on a 4-12% polyacrylamide gel, transferred and incubated simultaneously with an anti-GFP and the anti-BIP as loading control. Induction times are shown at the bottom. The total amount of YFP::IFT81 ("YFP", **expected molecular weight 113 kDa**) follows that of the loading control ("BIP", **expected molecular weight 71 kDa**) and is not affected by IFT inhibition. **The position of molecular weight markers is indicated on the left. One representative gel out of two is shown.**

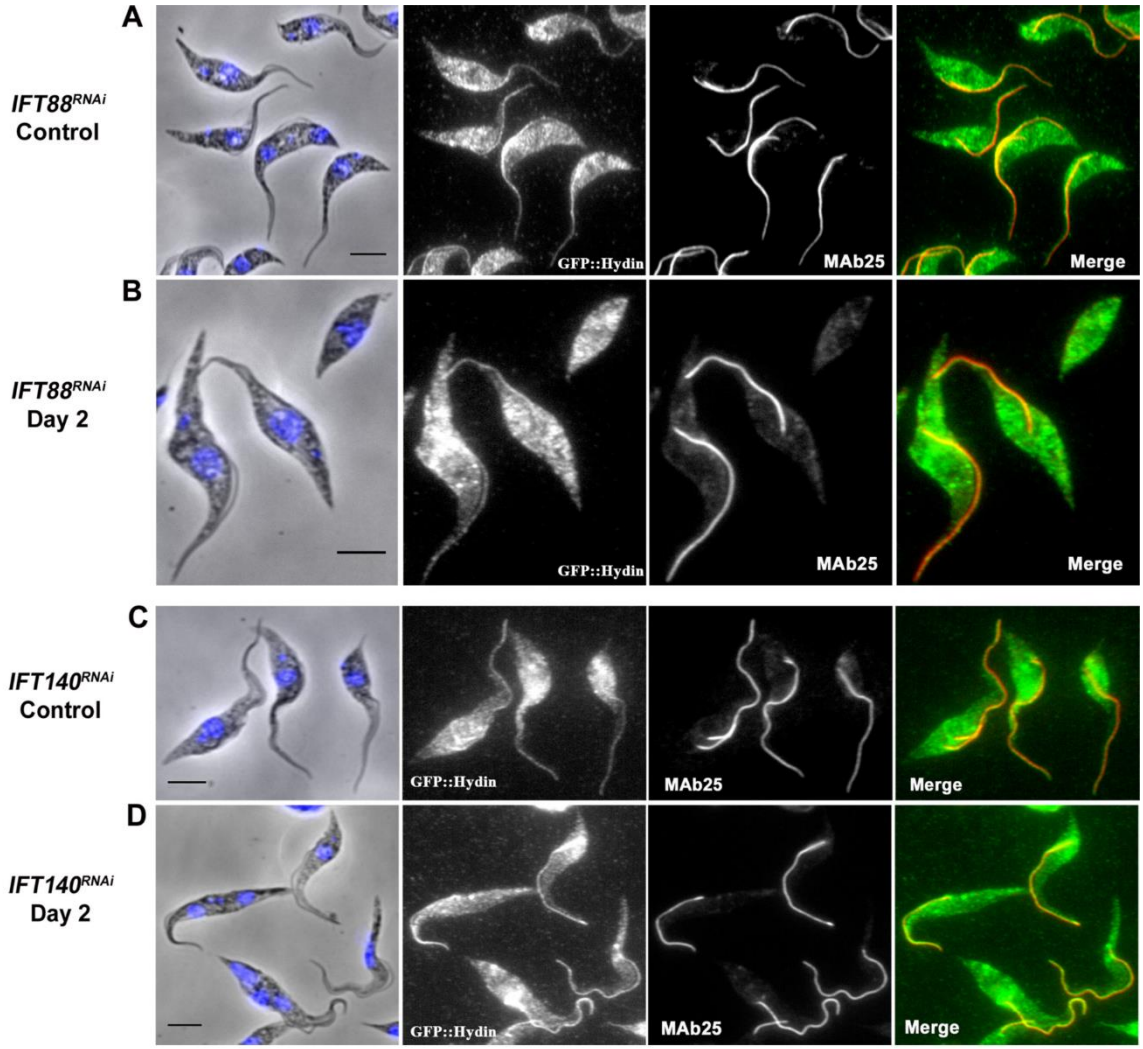


**Fig. S2**: Visualization of eGFP::Hydin distribution in *IFT88*$^{RNAi}$ (A-B) and *IFT140*$^{RNAi}$ (C-D) cells expressing eGFP::hydin from the endogenous locus. IFA was performed using the anti-GFP antibody to detect the fusion protein (white, green in merged panels), the anti-axoneme MAb25 antibody (red) and counterstained with DAPI (blue) in the indicated cell lines and conditions. The fusion protein is equally present along the whole length of flagellum in both induced and non-induced conditions. Bar, 5 µm.

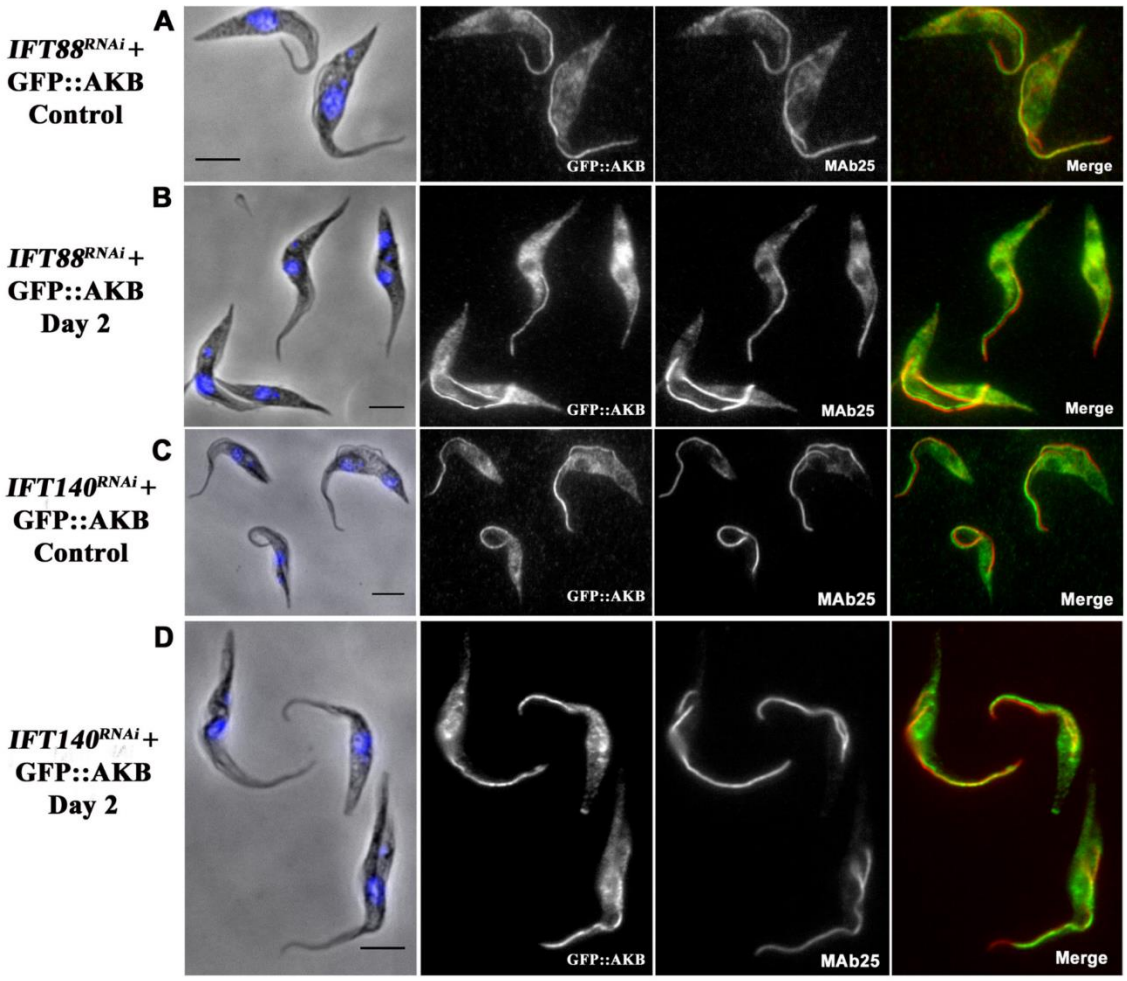


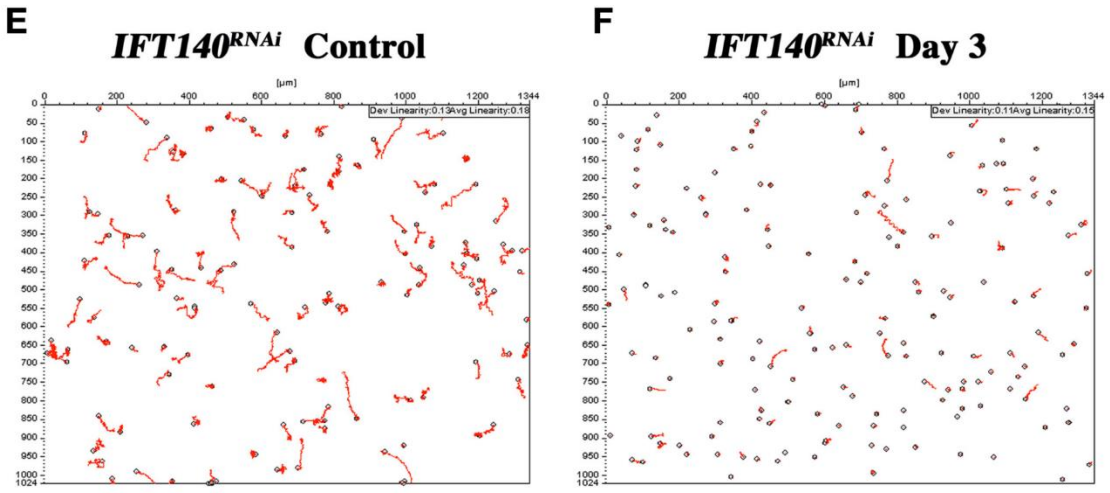

**Fig. S3:** Visualization of YFP::AKB protein in the old flagellum in *IFT88*$^{RNAi}$ (A-B) and *IFT140*$^{RNAi}$ (C-D) cells. Trypanosomes have been fixed in methanol and stained with the anti-GFP antibody (white, green in merged panels), the anti axoneme MAb25 antibody (white, red in merged panels) and DNA was stained with DAPI (in blue). YFP::AKB protein is slightly shifted from the axoneme signal as expected for a PFR protein. The fusion protein is equally present along the length of the PFR in both induced and non-induced conditions. Bar, 5 µm. **(E-F) Motility is arrested in induced *IFT140*$^{RNAi}$ cells. Velocities of control non-induced (left) and 3-day induced (right) *IFT140*$^{RNAi}$ cells were monitored by cell tracking. Most cells showed little or no movement in the induced conditions (right) whereas sustained motility was observed in the control (left).**

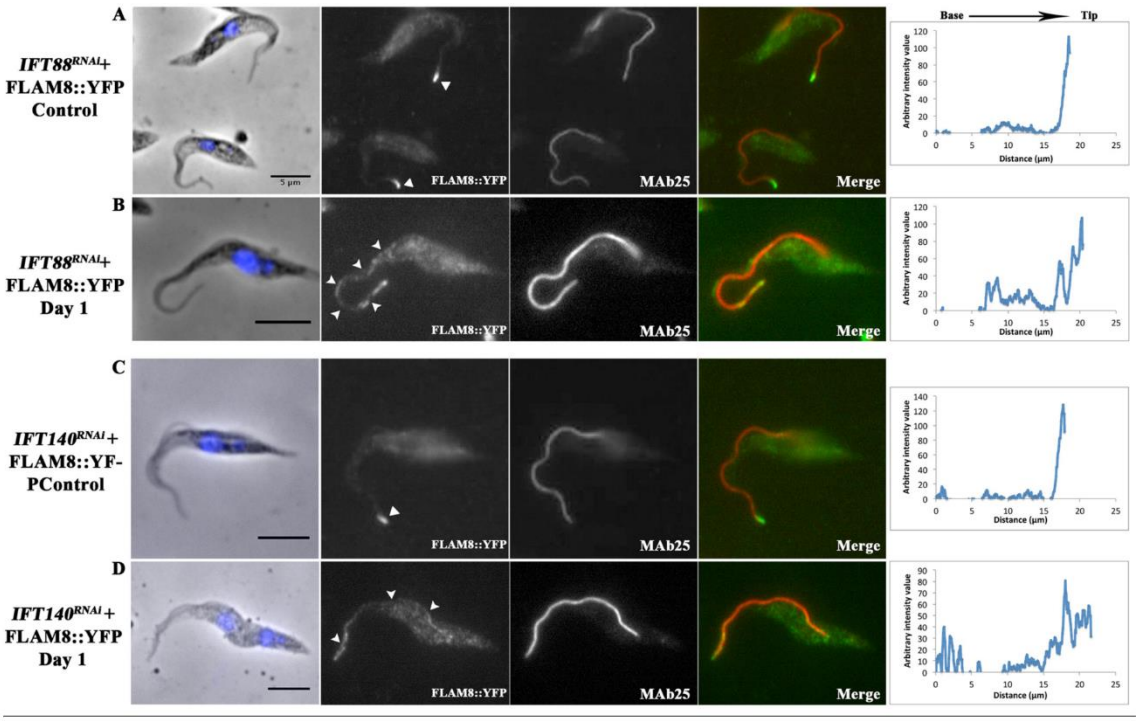


**Fig. S4**: Visualization of FLAM8 in whole *IFT88*$^{RNAi}$ (A-B) and *IFT140*$^{RNAi}$ (C-D) cells. IFA was performed using a rabbit anti-FLAM8 antibody (white and green in merge), the anti axoneme MAb25 antibody (white, red in merged panels) and counterstained with DAPI (blue) in the indicated cell lines and conditions. White arrowheads indicate the presence of FLAM8 at the tip of flagella (A, C) or along their length in induced *IFT88*$^{RNAi}$ and *IFT140*$^{RNAi}$ cells (B, D). Bar, 5 µm. Right, one-axis projections show the intensity of the signal along the length of the flagellum.


**Movie S1:** Visualisation of YFP::IFT81 in non-induced *IFT88*$^{RNAi}$ cells.

Live, time-lapse fluorescence microscopy of YFP::IFT81 in non-induced *IFT88*$^{RNAi}$ cells. Robust IFT is visible. All acquisitions were made at room temperature with frames taken every 100 ms for 30 sec. Videos were exported to .AVI format with the ImageJ 1.47e software.

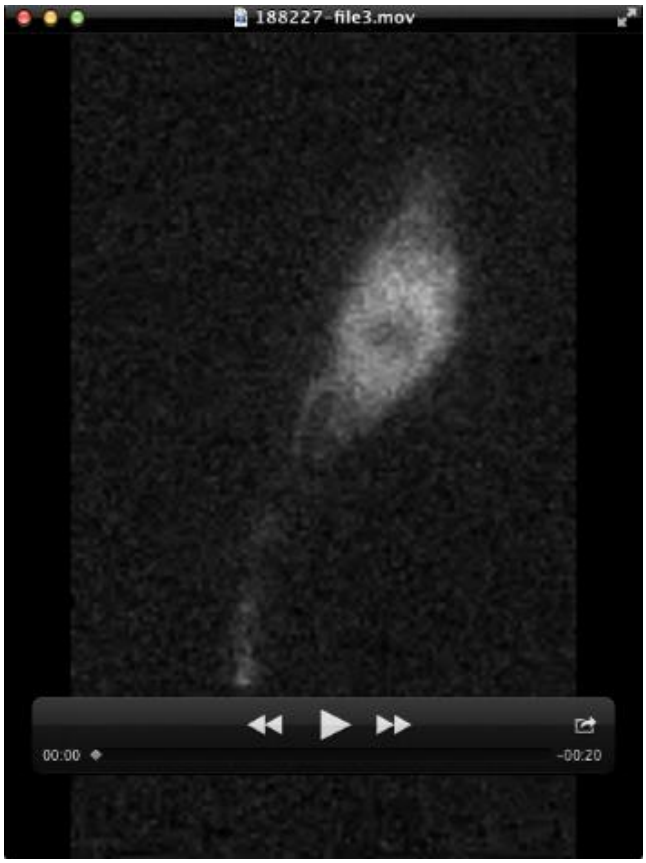


**Movie S2:** Visualisation of YFP::IFT81 in *IFT88*$^{RNAi}$ cells after two days of induction. Live, time-lapse fluorescence microscopy of induced YFP::IFT81 in *IFT88*$^{RNAi}$ cells. No trafficking is detected. All acquisitions were made at room temperature with frames taken every 100 ms for 30 sec.


**Movie S3:** Visualisation of YFP::IFT81 in non-induced *IFT140*$^{RNAi}$ cells.

Live, time-lapse fluorescence microscopy of non-induced YFP::IFT81 in *IFT140*$^{RNAi}$ cells. Robust IFT is visible. All acquisitions were made at room temperature with frames taken every 100 ms for 30 sec.


**Movie S4:** Visualisation of YFP::IFT81 in *IFT140*$^{RNAi}$ cells after 53h of induction.

Live, time-lapse fluorescence microscopy of induced YFP::IFT81 in *IFT140*$^{RNAi}$ cells. IFT signal accumulates towards the end of the flagellum. All acquisitions were made at room temperature with frames taken every 100 ms for 30 sec.


**Movie S5:** Visualisation of YFP::IFT81 in *IFT140*$^{RNAi}$ cells after 53h of induction.

Live, time-lapse fluorescence microscopy of induced YFP::IFT81 in *IFT140*$^{RNAi}$ cells. IFT signal strongly accumulates towards the end of the flagellum. All acquisitions were made at room temperature with frames taken every 100 ms for 30 sec.


**Movie S6:** Visualisation of YFP::IFT81 in *IFT140*$^{RNAi}$ cells at 53h of induction.

Live, time-lapse fluorescence microscopy of induced YFP::IFT81 in *IFT140*$^{RNAi}$ cells. A gradient of IFT signal is observed from the tip to the base of the flagellum. All acquisitions were made at room temperature with frames taken every 100 ms for 30 sec.


**Movie S7:** Visualisation of YFP::IFT81 in *IFT140*$^{RNAi}$ cells after 53h of induction.

Live, time-lapse fluorescence microscopy of induced YFP::IFT81 in *IFT140*$^{RNAi}$ cells following photobleaching (time 5s). All acquisitions were made at room temperature with frames taken every 100 ms for 30 sec.


**Movie S8:** Visualisation of YFP::IFT81 in *IFT140*$^{RNAi}$ cells after 53h of induction.

Live, time-lapse fluorescence microscopy of induced YFP::IFT81 in *IFT140*$^{RNAi}$ cells following photobleaching (time 5s). All acquisitions were made at room temperature with frames taken every 100 ms for 30 sec.